

# TeV $\gamma$ -rays and neutrinos from photo-disintegration of nuclei in Cygnus OB2

Luis A. Anchordoqui,<sup>1</sup> John F. Beacom,<sup>2</sup> Haim Goldberg,<sup>3</sup> Sergio Palomares-Ruiz,<sup>4,5</sup> and Thomas J. Weiler<sup>4</sup>

<sup>1</sup>*Department of Physics, University of Wisconsin-Milwaukee, P.O. Box 413, Milwaukee, WI 53201*

<sup>2</sup>*CCAPP, Departments of Physics and Astronomy, Ohio State University, Columbus, OH 43210*

<sup>3</sup>*Department of Physics, Northeastern University, Boston, MA 02115*

<sup>4</sup>*Department of Physics and Astronomy, Vanderbilt University, Nashville, TN 37235*

<sup>5</sup>*Institute for Particle Physics Phenomenology, University of Durham, Durham DH1 3LE, UK*

TeV  $\gamma$ -rays may provide significant information about high energy astrophysical accelerators. Such  $\gamma$ -rays can result from the photo-de-excitation of PeV nuclei after their parents have undergone photo-disintegration in an environment of ultraviolet photons. This process is proposed as a candidate explanation of the recently discovered HEGRA source at the edge of the Cygnus OB2 association. The Lyman- $\alpha$  background is provided by the rich O and B stellar environment. It is found that (1) the HEGRA flux can be obtained if there is efficient acceleration at the source of lower energy nuclei; (2) the requirement that the Lorentz-boosted ultraviolet photons can excite the Giant Dipole Resonance implies a strong suppression of the  $\gamma$ -ray spectrum compared to an  $E_\gamma^{-2}$  behavior at energies  $\lesssim 1$  TeV (some of these energies will be probed by the upcoming GLAST mission); (3) a TeV neutrino counterpart from neutron decay following helium photo-disintegration will be observed at IceCube only if a major proportion of the kinetic energy budget of the Cygnus OB2 association is expended in accelerating nuclei.

## I. INTRODUCTION

There are two well-known mechanisms for generating TeV  $\gamma$ -rays in astrophysical sources [1]. The first involves purely electromagnetic (EM) processes, including synchrotron emission and inverse Compton scattering. The second may be termed hadronic, in which the  $\gamma$ -rays originate in  $\pi^0$  decays. The latter can in turn be traced to either  $pp$  or  $p\gamma$  collisions.

The EM processes originate in the acceleration of electrons; as a result, the TeV  $\gamma$ -rays must be accompanied by an X-ray counterpart. In addition, the conflicting requirements on the magnetic field (large field for acceleration, small field for limiting synchrotron cooling) limits the energy of the emitted photons  $E_\gamma \lesssim 10$  TeV.

The hadronic  $p\gamma$  mode is characterized by a large threshold for  $\pi^0$  production, and thus it is favored only in very hot photon environments, or in the presence of very energetic proton beams. In addition, the presence of the high threshold allows acceleration free of scattering losses as long as the Hillas criterion [2] holds. In the  $pp$  hadronic mode, threshold effects are insignificant. Because of this, it is generally assumed that  $\pi^0$  production occurs in a region distinct from the site of the primary acceleration. However, one can set conditions relating the interaction length of the nucleons, the neutron decay lifetime and the source confinement radius to permit simultaneous emission of neutrons,  $\gamma$ -rays and neutrinos [3]. In the  $p\gamma$  mode the spectrum of  $\gamma$ -rays follows that of the parent proton population in the energy region above threshold. In the  $pp$  mode, the resulting  $\gamma$ -ray spectrum is broad, reflecting the presence of a quasi-Feynman plateau which spans the entire rapidity space. The photon spectrum will deviate from the proton spectrum if the Feynman plateau is not flat in rapidity space [4], as suggested by Tevatron data [5]. Finally, for both the  $p\gamma$  and  $pp$  modes, the decay of the charged pions yield a neutrino counterpart

with energy and intensity similar to the photons.

In this paper, we discuss in detail a third dynamic which can lead to TeV  $\gamma$ -rays: the photo-disintegration of nuclei at the source, followed by the photo-de-excitation of the daughter nuclei [6]. In order to generate TeV  $\gamma$ -rays as a result of emission of MeV  $\gamma$ -rays in the rest frame of the de-exciting nucleus, the Lorentz factor of the boosted nucleus must be  $\sim 10^6$ . For this boost factor, excitation via the Giant Dipole Resonance ( $\sim 10$  MeV – 30 MeV in the nucleus rest frame) is obtained with ambient photons with energies in the far ultraviolet (usually defined as 1-20 eV). Photons of these energies are expected from the Lyman  $\alpha$  emissions from hot stars. This process clearly reduces the threshold energy requirement relative to  $p\gamma$ . The important role played by the Giant Dipole Resonance (GDR) in the photo-disintegration effectively suppresses the  $\gamma$ -ray spectrum below 1 TeV.

In recent decades, the Cygnus Spiral Arm has been a site of  $\gamma$ -ray signal candidates which tend to come and go. In the energy band  $2 \times 10^6 < E_\gamma/\text{GeV} < 2 \times 10^7$ , data collected by the Kiel air shower experiment [7] show a  $4.4\sigma$  excess of events in the direction of the binary system Cygnus X-3, with the typical 4.8 hr modulation previously observed in the MeV [8] and TeV [9] regions. This result, including the X-ray binary period, was later confirmed by the Haverah Park data [10], with the additional observation of an abrupt steepening of the spectrum at  $E_\gamma > 2 \times 10^7$  GeV. The distance ( $\approx 10$  kpc) to Cygnus X-3 slightly exceeds the minimum path length for cosmic microwave background (CMB) absorption in the energy band of the Kiel experiment [11]. However, since absorptive effects decrease for energies beyond  $10^7$  GeV (see Fig. 1), the observed steepening must be traced to a softening of the injection spectrum.

At a much higher energy  $\gtrsim 5 \times 10^8$  GeV, the analysis of the cumulative Fly's Eye data also revealed an excess of events from the direction of Cygnus X-3, with chance

probability of  $6.5 \times 10^{-4}$  [12]. A  $3.5\sigma$  excess from this direction and in the same energy region has also been observed at the Akeno air shower array [13]. The inferred signal fluxes are consistent at the  $1\sigma$  level. However, the evidence for the 4.8 hr modulation is termed as “weak” by the Fly’s Eye Collaboration, and is absent in the Akeno data. Thus, one may infer that the high energy signals originate in a different source within the angular field of view of Cygnus X-3.

More recent data from the CASA-MIA [14] and the HEGRA [15] experiments place restrictive bounds on steady state fluxes from the Cygnus region. These can be seen in Fig. 1, and suggest that the earlier reported fluxes do not reflect current steady state activity. At this point, it is critical to note that only the HEGRA experiment has the angular resolution to place an upper limit on the steady state flux from Cygnus X-3, and at the same time observe significant activity (at the  $7\sigma$  level) in the TeV region from an unidentified source (with no optical or X-ray counterparts) which is within  $0.5^\circ$  of the X-ray binary [15]. An excess at the  $3.3\sigma$  level from the direction of this unidentified source is also present in the Whipple data [16]. The strength and specificity of the source, and the distinct absence of an X-ray counterpart, make this source a good candidate for probing the nucleus photo-disintegration/de-excitation model for producing TeV  $\gamma$ -rays.

Especially intriguing is the possible association of the TeV HEGRA source with Cygnus OB2, a cluster of several thousands of young hot OB stars. At a relatively small distance ( $\approx 5000$  light years) to Earth, this is the largest massive Galactic stellar association. Cosmic ray nuclei are expected to be trapped and accelerated through turbulent motions and collective effects of star winds. In this paper we present a model for explaining the HEGRA observations, in which the trapped high energy nuclei undergo stripping on the starlight background and their surviving fragments emit  $\gamma$ -rays in transition to their ground states. A short version highlighting the salient features of the model has been issued as a companion paper [17]. The outline here is as follows: in Sec. II we provide a detailed description of the salient characteristics of the Cygnus OB2 association, including stellar counts, lifetime, size and energy considerations. Section III contains a description of the HEGRA TeV source, and summarize the different proposed explanations. The model is presented in Sec. IV, including a calculation of the TeV photon flux, following a discussion of the accompanying neutrino flux. In Sec. V we compare the TeV  $\gamma$ -ray and neutrino yields in the model with those corresponding to the hadronic modes. In Sec. VI we examine the possibility whether our model can accommodate the emission of ultra-high energy cosmic rays. Conclusions are collected in Sec. VII.

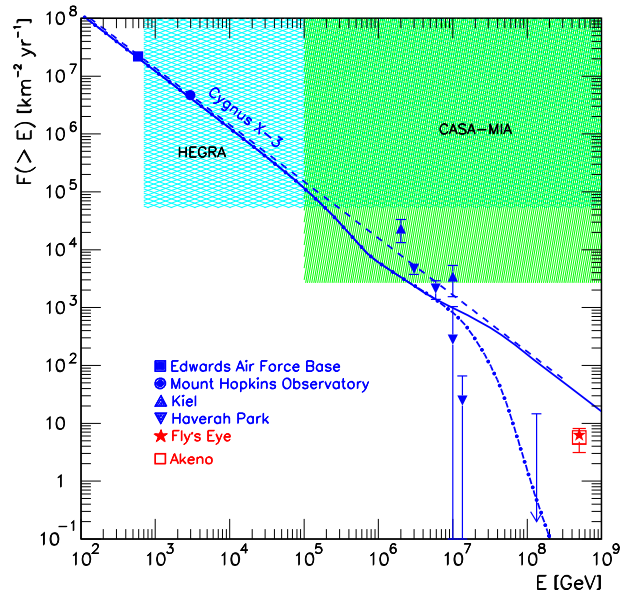


FIG. 1: Integrated flux from the binary system Cygnus X-3 as reported by the different collaborations. The dotted line is a best single power law fit,  $F_\gamma(> E_\gamma) = 3.3 \times 10^{-8} (E_\gamma/\text{GeV})^{-0.98} \text{ cm}^{-2} \text{ s}^{-1}$ , to the Cygnus X-3 data:  $\blacktriangle$  [7],  $\blacksquare$  [9],  $\bullet$  [9], and  $\blacktriangledown$  [10]. The accompanying solid and dash-dotted lines take into account attenuation on the CMB, with the latter also including a cutoff at the source. Also shown are the integrated fluxes of neutral particles from the direction of Cygnus X-3 reported by the Akeno ( $\square$  [13]) and Fly’s Eye ( $\star$  [12]) collaborations. The cross-hatched bands indicate the 90% CL upper limit on steady state flux from the direction of Cygnus X-3 as observed by the CASA-MIA [14] and HEGRA [15] experiments.

## II. CYGNUS OB2 IN A NUTSHELL

The Cygnus OB2 (VI Cygni) association is one of the most massive associations, with some of the most luminous stars, in our Galaxy. It was first noticed by Münch and Morgan [18] who, during the course of a classification of blue giants (OB stars), found eleven of these objects in that region. Since the pioneering spectroscopy and photometry of Johnson and Morgan [19] and subsequent works [20], this region has been known to harbor a large population of massive and early type stars, which have been found to be highly reddened. The first comprehensive study of this stellar association [21, 22, 23] identified a few hundred OB stars as possible members based on photographic photometry. Other photometric and spectroscopic studies [24] were carried out during following years confirming and extending the first results.

Cygnus OB2 is located at galactic coordinates  $(l, b) \sim (80^\circ, 1^\circ)$ , behind the Great Cygnus Rift. The study performed in Ref. [22], inferred an elliptical shape with major and minor axes of  $48'$  and  $28'$ , respectively, and esti-

mated more than 3000 stars with at least 300 of OB spectral type, which resulted in a total mass for the association of  $(0.6 - 2.7) \times 10^4 M_\odot$ . However, due to the extreme reddening in and around this region, which hampers the detection of even OB stars, the observed morphology was rather an artifact created by the particular extinction pattern of the field. A more recent work [25] based on a statistical study of point sources revealed by the *Two Micron All Sky Survey* (2MASS) in the near-infrared, shows that this association is much larger and richer than previously thought. The resulting stellar distribution reveals a rather regular and almost circular density profile with the center located at  $(\alpha, \delta) = (20^h 33^m 10^s, +41^\circ 12')$  and with a pronounced maximum slightly offset at  $(\alpha, \delta) = (20^h 33^m 10^s, +41^\circ 15.7')$ . Stars counts show that 50% of the members are located within a radius of  $21'$ , and 90% within a radius of  $45'$  around the center, merging with the field stars at a radius of  $\sim 1^\circ$ . The central stellar density reaches 4.5 stars/arcmin<sup>2</sup> above the field star density, and drops to 50% at a radius of  $13'$ . By integrating the radial density profile, after subtraction of the field star density, the total number of OB stars was found to be  $2600 \pm 400$  [25], much larger than the earlier estimate of  $\sim 300$  [22]. Furthermore, the total number of O-type stars was inferred to be  $120 \pm 20$  [25]. Nevertheless, this number must be cast as an upper limit, as the 2MASS data do not allow a precise spectral determination and hence do not account for possible evolutionary effects, i.e., the quoted number reflects the initial number of very massive ( $\gtrsim 20 M_\odot$ ) stars, although some may have already evolved. This also agrees with more recent estimates [26, 27] and suggests a total mass for the association of  $(4 - 10) \times 10^4 M_\odot$ , where the primary uncertainty comes from the unknown lower mass cut-off. Using the radial density profile, a central mass density of  $(40 - 150) M_\odot/\text{pc}^3$  is determined [25].

Early distance determinations revealed the proximity of this region, varying from 1.5 kpc [19] to 2.1 kpc [22]. More recent estimates have set this distance to  $d \sim 1.7$  kpc [28, 29]. At such distance, the inner  $21'$ , with half the total number of objects, results in a physical radius of  $R_{\text{in}} \sim 10$  pc, with  $R_{\text{out}} \sim 30$  pc being the radius of the association. Yet, a revision of the effective temperature scale of O-type stars yields a closer distance of  $\sim 1.5$  kpc [27], when the age of the association is taken into account in fitting the late-O and early-B dwarfs to model isochrones. It is from the superposition of the isochrones (calculated using the theoretical evolutionary tracks of the model of Ref. [30]) on the Hertzsprung-Russell diagrams, that the age of the association has been estimated to lie between 1–4 Myr [31], compatible with other estimates [27, 28, 32, 33]. This range reflects the dispersion of the upper main sequence and agrees with the fact that the observed large number of O-type stars implies that the association should be younger than  $\sim 5$  Myr, because in the case of coeval star formation, the number of this type of stars decreases rapidly [31]. In addition, the fact that there are some Wolf-Rayet stars within Cygnus OB2

suggests an age larger than  $\sim 2$  Myr. On the other hand, the non-detection of any supernova remnant in Cygnus OB2 [34] points to an association younger than  $\sim 4$  Myr. Nevertheless, the presence of a few slightly evolved supergiants (an O3 If\* star, three Wolf-Rayet stars and two LBV candidates) suggests that the star formation in the association was not strictly coeval and there are even indications of ongoing star formation [28, 29, 33, 35, 36]. This fact would narrow down the quoted age boundaries.

Early estimates of the wind mechanical luminosity for the Cygnus OB2 association gave  $L_w \simeq 10^{38} \text{ erg s}^{-1}$  [32]. However, the improved data on the population of the region required a revision of this estimate. By using a detailed analysis of radiatively wind models for hot stars, it has been shown that at an early stage ( $\lesssim 2$  Myr), the wind mechanical luminosity is maintained approximately constant [37], being  $\sim 2 \times 10^{34} \text{ erg s}^{-1}$  per solar mass, which, for the association, yields  $L_w \simeq (1 - 2) \times 10^{39} \text{ erg s}^{-1}$  [38]. After the first  $\sim 2$  Myr, the luminosity increases further as Wolf-Rayet stars appear. This estimate assumes stars of solar metallicity and a Salpeter initial mass function (IMF) slope. There have been different calculations for the IMF slopes [25, 29, 31, 35] which however do not agree with each other, although lie in the interval  $\Gamma \simeq -(1.0 - 1.6)$  ( $\Gamma_S = -1.35$  being the Salpeter slope). Nevertheless, these discrepancies are due to systematic uncertainties and hence, a reasonable approximation is to assume a uniform canonical Salpeter slope. Should the metallicity be close to the solar value, this implies [37] that the estimate of the wind mechanical luminosity is probably correct within a factor of  $\sim 2$ . Other values for the metallicity would modify this prediction by at most a factor  $\lesssim 10$ . On the other hand, the total Lyman continuum luminosity of the stars has been estimated to be  $\sim 10^{51} \text{ photons s}^{-1}$  [31].

Recently, there have been observations of TeV  $\gamma$ -rays from the northeast boundary of this association (see Fig. 2) [15]. These observations will be discussed in the following section, and will constitute the focus of this paper.

### III. TeV J2032+4130

The HEGRA system of Imaging Atmospheric Čerenkov Telescopes (HEGRA IACT-system) consisted of five identical Čerenkov telescopes (each with  $8.5 \text{ m}^2$  mirror area) and employed a stereoscopic technique achieving an angular and energy resolution better than  $0.1^\circ$  and 15%, respectively, for  $\gamma$ -rays on an event-by-event basis with energies from 0.5 TeV to  $\sim 50$  TeV [39].

The observation of the Cygnus region by the HEGRA IACT-system has allowed the serendipitous discovery of a TeV source in the outskirts of the core of Cygnus OB2 [40]. The analysis of the total 278.3 hours of observations performed in two periods from 1999 to 2002 (120.5 hours from 1999 to 2001 [40] and 157.8 hours dur-

ing 2002 [15]) has revealed the presence of a steady (and possibly extended) TeV source, with hard injection spectrum. Interestingly, there have been earlier claims of a multi-TeV excess in this region [41].

The excess significance of the TeV source is  $7.1\sigma$  and it appears extended at more than  $4\sigma$  level with a morphology which is suitably described by a Gaussian profile. The source is termed TeV J2032+4130 after the position of the center of gravity. Its extension (Gaussian  $1\sigma$  ra-

dius) is  $6.2'(\pm 1.2'_{\text{stat}} \pm 0.9'_{\text{sys}})$ , which at a distance of 1.7 kpc results in  $r \sim 3.07(\pm 0.59_{\text{stat}} \pm 0.45_{\text{sys}})$  pc.

Three different types of intrinsic morphology were tested [15] (disc, volume and surface), but the data cannot discriminate between them. The energy spectrum determination yielded a pure power-law fit with a hard photon index, showing no indication for an exponential cut-off, given by [15]

---


$$\frac{dF_\gamma}{dE_\gamma} = 6.2(\pm 1.5_{\text{stat}} \pm 1.3_{\text{sys}}) \times 10^{-13} \left(\frac{E_\gamma}{\text{TeV}}\right)^{-1.9(\pm 0.1_{\text{stat}} \pm 0.3_{\text{sys}})} \text{cm}^{-2}\text{s}^{-1}\text{TeV}^{-1} \equiv N_{\text{HEGRA}} \left(\frac{E_\gamma}{\text{TeV}}\right)^{-\alpha_{\text{HEGRA}}}, \quad (1)$$


---

which implies a flux above 1 TeV given by

$$F_\gamma(E_\gamma > 1\text{TeV}) = 6.9(\pm 1.8_{\text{stat}}) \times 10^{-13} \text{cm}^{-2}\text{s}^{-1}. \quad (2)$$

These results imply a luminosity of  $\sim 10^{32}$  erg/s above 1 TeV, which is well within the kinetic energy budget of Cygnus OB2, and indeed, also within that of a number of notable member stars [29, 43].

As can be seen in Fig. 2, this signal is located at the edge of the error circle of the EGRET source 3EG J2033+4118 and within the  $\sim 10$  pc-radius core circle of the Cygnus OB2 association. The EGRET observations [45] lie in the energy range below 10 GeV, and closely display a spectrum  $\propto E_\gamma^{-2}$ . It will be of important significance for our discussion that when extrapolated to the TeV range according to the  $E_\gamma^{-2}$  behavior, the flux exceeds the HEGRA flux by several orders of magnitude. Hence we surmise that these observations constitute two different sources.

An additional set of observations performed during 1989-90 by the Whipple Observatory atmospheric Čerenkov imaging telescope [16] has been recently re-analyzed in the light of the HEGRA data. These confirm an excess in the same direction as J2032+4130, although with considerably larger flux, above a peak energy energy response of 0.6 TeV. The statistical significance of the signal is only 10% smaller with selection of events above 1.2 TeV. However, the large differences between the flux levels cannot be explained as errors in estimation of the sensitivity of the experiments since they have been calibrated by the simultaneous observations of other TeV sources.

So far no clear counterparts at other wavelengths have been identified, and moreover, the observed spectrum is not easily accommodated with synchrotron radiation by electrons [40]. The difficulty to accommodate the spectrum by conventional electromagnetic mechanisms has been exacerbated by the failure of CHANDRA and VLA to detect X-rays or radiowaves signaling acceleration of any electrons [44].

Nevertheless, a leptonic origin is not yet excluded, es-

pecially if the TeV source is actually located in the vicinity of Cygnus X-3. The suggested model [40] proposes a jet-driven termination shock at the boundary where the relativistic jet meets the interstellar medium. This results in synchrotron and TeV inverse-Compton emission from the accelerated electrons [46], giving rise to the observed signal. Such a jet could emanate either from an as-yet undiscovered microquasar or from Cygnus X-3. Interestingly, the TeV signal aligns well with the northern error cone of the bi-lobal jet of Cygnus X-3 [47]. For the observed angular separations, this would place the TeV source at a distance of 10 kpc from Earth, and around 70 pc from Cygnus X-3.

The fact that there is no catalogued X-ray sources within the  $2\sigma$  error circle of the TeV source would disfavor a leptonic origin at Cygnus OB2. We now briefly discuss some models in which accelerated protons and nuclei interacting with a local dense gas cloud [44] or with stellar winds [48], produce photons from  $\pi^0$  decay. In the case of gas cloud interactions [44], an interstellar density of  $n_{\text{tot}} \sim 30 \text{cm}^{-3}$  and an injection efficiency (the ratio of cosmic ray energy to the kinetic energy of the accelerating winds) of 0.08% reproduces well the observed TeV spectrum. However, such a large density has been called into question [48] because a re-assessment [49] of the CO-H<sub>2</sub> conversion factor for this type of environment (used for calibration) would imply a considerably lower density,  $n_{\text{tot}} \sim 0.1 \text{cm}^{-3}$ . With such a density, a much larger injection efficiency  $\sim 25\%$  would be required. A different model in terms of cosmic ray illumination of stellar winds has been suggested to explain the signal through hadronic interactions in the innermost parts of the winds of massive OB stars [48]. However, a more recent detailed study of the stellar winds [50], including pressure effects and a more accurate estimate of the (lower) mass-loss rate for OB stars, resulted in a significant reduction in the photon emission rate. Thus, if only the currently known stars exist, the predicted flux from this model is too low to comfortably explain the TeV source.

Another suggested possibility has been that of a point-

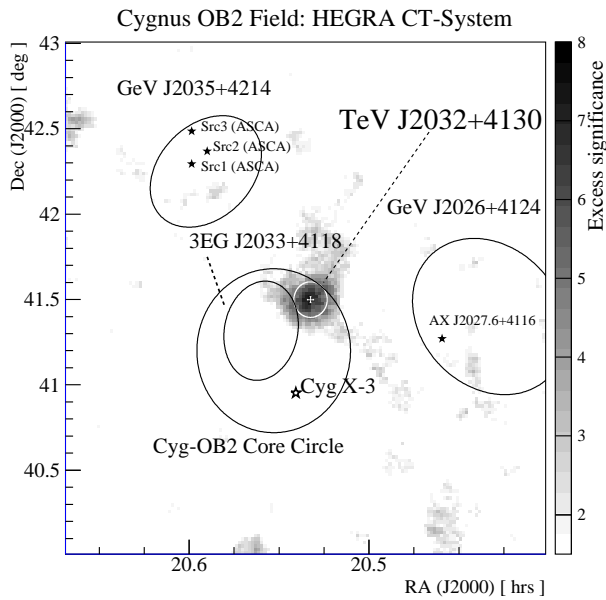


FIG. 2: Skymap of correlated event excess significance ( $\sigma$ ) from all HEGRA IACT-System data ( $3^\circ \times 3^\circ$  FoV) centered on the TeV source J2032+4130. Nearby objects are also shown: 95% contours for 3 EGRET sources (indicated by the ovals), their possible X-ray associated counterparts (as given in Ref. [42]), and Cygnus X-3. The center of gravity with statistical errors and intrinsic size (standard deviation of a 2-dim Gaussian,  $\sigma_{src}$ ) are indicated by the white cross and white circle, respectively. The TeV source, J2032+4130, is positioned at the edge of the error circle of the EGRET source 3EG J2033+4118, and within the core circle of the extremely dense OB stellar association Cygnus OB2 [15].

like origin of the TeV signal related to an unusual transient X-ray source which lies  $7'$  from the center of gravity of TeV J2032+4130 [51]. However, the position and variability of this X-ray source and mainly, the confirmed extension of the TeV source makes this a remote alternative, although it remains possible that several point-like TeV sources could be masquerading as a single extended source.

The TeV signal could also be interpreted as originated in the wind nebulae of an as-yet undetected recent pulsar (similar to Vela-type pulsars), as a result of hadronic or leptonic interactions [52]. This pulsar must have been formed  $\sim 10^4$  years ago in a core collapse of one of the massive stars in the Cygnus OB2 association. However, the non-observation of any supernova remnant in the region, as well as the greatly lowered estimates of the ambient gas density, seem to pose a serious challenge for this model.

In summary, there is no single compelling explanation for the various characteristics of TeV J2032+4130 [53]. In the next section, we present a new mechanism for explaining the HEGRA data.

## IV. THE MODEL

There are two processes by which the nucleus may produce  $\gamma$ -rays, photo-disintegration of the nucleus by ambient photons followed by de-excitation of a daughter nucleus, and photo-pion production followed by decay of the neutral pions. The two processes have different thresholds and different signatures. In this section, we are concerned with the former mechanism, emphasized more than a decade ago by Moskalenko and collaborators [54], but largely ignored by the rest of the  $\gamma$ -ray community. In the following section we will compare and contrast the two processes.

### A. Nucleus Photo-Disintegration

The interaction between photons and high energy nuclei results in the emission of nucleons. The relevant photonuclear interaction process for the relevant energies have been studied from the point of view of the collective and the shell models [55]. It is shown that collective nuclear states dominate the interaction, with low angular momentum modes preferred. In the energy region which extends from threshold for single-nucleon emission  $\sim 10$  MeV up to  $\sim 30$  MeV the GDR dominates. The GDR typically de-excites by the statistical emission of a single nucleon. Above the GDR region, and up to the photo-pion production threshold at  $E_{th}^\pi = m_\pi (1 + m_\pi/2m_N) \simeq 145$  MeV, the non-resonant processes provide a much smaller cross section with a relatively flat dependence on energy.

The photo-disintegration rate for a highly relativistic nucleus with energy  $E = \gamma A m_N$  (where  $\gamma$  is the Lorentz factor) propagating through an isotropic photon background with energy  $\epsilon$  and spectrum  $n(\epsilon)$ , normalized so that the total number of photons in a box is  $\int n(\epsilon) d\epsilon$ , is [56]

$$R_A = \frac{c}{\lambda_A} = \frac{1}{2} \int_0^\infty \frac{n(\epsilon)}{\gamma^2 \epsilon^2} d\epsilon \int_0^{2\gamma\epsilon} \epsilon' \sigma_A(\epsilon') d\epsilon', \quad (3)$$

where  $\sigma_A(\epsilon')$  is the cross section for photo-disintegration of a nucleus of mass  $A$  by a photon of energy  $\epsilon'$  in the rest frame of the nucleus.

The cross section for all the different nuclear species has been obtained through a direct fit to data [57]. For medium and heavy nuclei ( $A \geq 30$ ) the total photon absorption cross section can be approximated by a dipole form (sometimes called a ‘‘Breit-Wigner’’ or ‘‘Lorentzian’’)

$$\sigma_A(\epsilon') = \sigma_0 \frac{\epsilon'^2 \Gamma^2}{(\epsilon_0'^2 - \epsilon'^2)^2 + \epsilon'^2 \Gamma^2}, \quad (4)$$

where  $\Gamma$  is the width,  $\epsilon_0'$  is the central value of the GDR energy band, and  $\sigma_0$  is the normalization. We have found that for the considerations in the present work, the cross

section can be safely approximated by the single pole of the Narrow-Width Approximation,

$$\sigma_A(\epsilon') = \pi \sigma_0 \frac{\Gamma}{2} \delta(\epsilon' - \epsilon'_0), \quad (5)$$

where  $\sigma_0/A = 1.45 \times 10^{-27} \text{cm}^2$ ,  $\Gamma = 8 \text{ MeV}$ , and  $\epsilon'_0 = 42.65A^{-0.21} (0.925A^{2.433}) \text{ MeV}$ , for  $A > 4$  ( $A \leq 4$ ) [58, 59]. Inserting Eq. (5) into Eq. (3) we obtain

$$\begin{aligned} R_A &\approx \frac{\pi \sigma_0 \epsilon'_0 \Gamma}{4\gamma^2} \int_0^\infty \frac{d\epsilon}{\epsilon^2} n(\epsilon) \Theta(2\gamma\epsilon - \epsilon'_0) \\ &= \frac{\pi \sigma_0 \epsilon'_0 \Gamma}{4\gamma^2} \int_{\epsilon'_0/2\gamma}^\infty \frac{d\epsilon}{\epsilon^2} n(\epsilon). \end{aligned} \quad (6)$$

As a test of our approximation, we first compute the disintegration rate for a nucleus passing through a region where

$$n(\epsilon) = n_T^{\text{BE}}(\epsilon) = (\epsilon/\pi)^2 \left[ e^{\epsilon/T} - 1 \right]^{-1}, \quad (7)$$

corresponding to a Bose-Einstein distribution with temperature  $T$ . The result is

$$R_A^{\text{BE}} \approx \frac{\sigma_0 \epsilon'_0 \Gamma T}{4\gamma^2 \pi} \left| \ln \left( 1 - e^{-\epsilon'_0/2\gamma T} \right) \right|. \quad (8)$$

We then verify that for  $^{56}\text{Fe}$  and for the CMB temperature ( $T = 2.3 \times 10^{-4} \text{ eV}$ ), this solution agrees to within 20% with the parametrization given in [60]. The latter was derived using the full form of the cross section presented in [57]. (A similar result in the context of photo-disintegration of nuclei at the Galactic center has been obtained in [61].)

In the companion paper [17] it was argued that the rate can be written as a function  $w^2 |\ln(1 - e^{-w})|$  of a scaling variable  $w \equiv \epsilon'_0/2\gamma T$ , times a prefactor  $(\sigma_0 \Gamma/\epsilon'_0) T^3/\pi$ . The peak rate therefore scales as the prefactor. Using the fits mentioned below Eq. (5), the prefactor in turn scales in  $A$  as  $A^{1.21}$ , with a small correction for  $A \leq 4$  nuclei such as helium.

## B. The Photon Population

The ingredients necessary for calculating the total photo-disintegration rate from a given region of the OB association are (i) an ambient photon distribution in order to obtain the rate  $R_A^*$  on starlight per nucleon, and (ii) an initial population density of nuclei  $n_A$  in the region. In a qualitative manner, the iron (silicon) photo-disintegration rate in a region of radius  $R_{\text{in}} \approx 10 \text{ pc}$

$$\begin{aligned} \frac{dN}{dt} &= -N_{\text{Fe(Si)}} R_{56(28)}^* \\ &= -(4/3)\pi R_{\text{in}}^3 n_{\text{Fe(Si)}} R_{56(28)}^*, \end{aligned} \quad (9)$$

where  $n_{\text{Fe(Si)}}$  is the iron (silicon) population density in some energy bin. This population will be assumed to result from continuous trapping of the diffuse cosmic ray

flux by diffusion in a milligauss magnetic field [62], acting preferably on heavy nuclei. Energies of  $\mathcal{O}$  (PeV/nucleon) are achieved through re-acceleration in strong winds of the OB stars. We assume, and justify *a posteriori*, that the nucleus population  $n_{\text{Fe(Si)}}$  does not significantly change during the time considered. It will be seen below that *at most one nucleon will be stripped in the region of interest during the diffusion time within the association*; in the calculation of the disintegration rate, this justifies inclusion of only the lowest order in the photo-nuclear interaction.

The photon background will be assumed to result from the thermal emission of the stars in the region  $R$ . The average density in the region  $R$  will reflect both the temperatures  $T_O$  and  $T_B$  due to emission from O and B stars, respectively, and the dilution resulting from inverse square law considerations. Specifically, for a region with  $N_O$  O stars and  $N_B$  B stars, the photon density is

$$n^*(\epsilon) = \frac{9}{4} \left[ \frac{n_{T_O}^{\text{BE}}(\epsilon) N_O R_O^2 + n_{T_B}^{\text{BE}}(\epsilon) N_B R_B^2}{R^2} \right], \quad (10)$$

where  $R_{O(B)}$  is the radius of the O (B) stars, the factor 9/4 emerges when averaging the inverse square distance of an observer from uniformly distributed sources in a region  $R$  [63]. We take the O and B star populations to be 5% and 95%, respectively, of the total OB population of 2600 in the association. At this point, we do not differentiate between the 3 pc cell HEGRA hot spot and the rest of the cells in the association. In order to take into account the larger density of stars in the region of interest, we consider all the stars to lie within the central region,  $R = R_{\text{in}} \sim 10 \text{ pc}$ .

In Fig. 3 we show the dependence on the Lorentz factor of  $R_{56}^*$ ,  $R_{28}^*$ , and  $R_4^*$  for the stellar ambiance described above (solid lines). The peaks of the three rate curves, while occurring at slightly different values of  $\gamma$ , are seen to scale as  $A^{1.2}$ . This is in accord with our discussion of scaling below Eq. (8). Also in accord with our scaling formula, the positions in  $\gamma$  of the peak rates should scale in  $A$  as  $\gamma_{\text{peak}} \sim \epsilon'_0/w_{\text{peak}} \sim A^{-0.21}$ . The three curves bear this out. We have taken for the O (supergiants [64]) stars a surface temperature  $T_O = 40000 \text{ K}$ , and radius  $R_O = 19 R_\odot$ ; for the cooler B stars we assign  $T_B = 18000 \text{ K}$  and radius  $R_B = 8 R_\odot$  [27, 65]. For all three nuclei, the disintegration time exceeds the diffusion time ( $\sim 10^4 \text{ yr}$  [52]) of the nucleus in the association. Thus, the *a priori* assumption of a lowest order calculation has been justified [66].

At first sight this model might seem to be a very crude approximation of the actual distribution of stars. We have also calculated the photo-disintegration rate with a more detailed model of the star distribution. We consider the thermal emission to come from the stars in the whole association,  $R_{\text{out}} \sim 30 \text{ pc}$ , and that half of them are uniformly distributed in the inner region,  $R_{\text{in}} \sim 10 \text{ pc}$ , and the other half are uniformly distributed in the outer shell, i. e. the density of stars in the inner region is

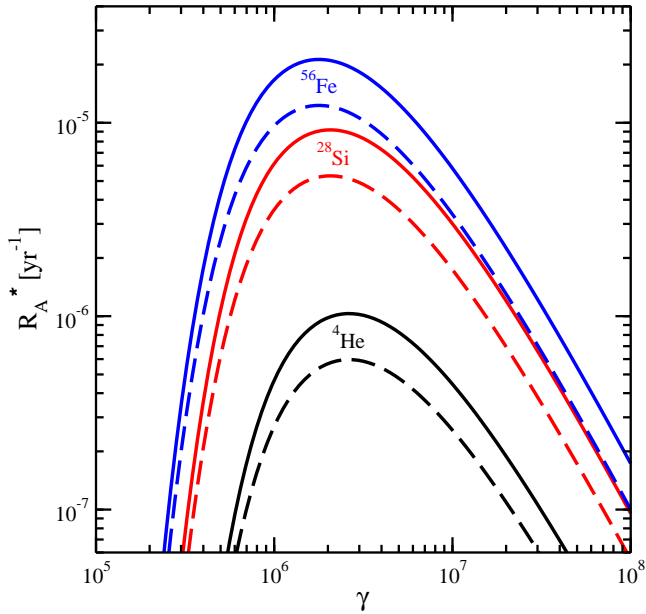


FIG. 3: Photo-disintegration rate of  $^{56}\text{Fe}$ ,  $^{28}\text{Si}$ , and  $^4\text{He}$  on the Cygnus OB2 starlight. Solid (dashed) lines represent the simplified (more elaborate) model as described in the text.

$(R_{\text{out}}/R_{\text{in}})^3 - 1 \sim 26$  times that in the outer shell. The photo-disintegration is calculated to occur in a region of radius  $r \sim 3$  pc in the outskirts of the inner part of the association,  $R_{\text{in}}$ , to model the size and position of the source of the HEGRA signal. This results in a photon density

$$n^*(\epsilon) = \frac{47}{4} \left[ \frac{n_{T_{\text{O}}}^{\text{BE}}(\epsilon) N_{\text{O}} R_{\text{O}}^2 + n_{T_{\text{B}}}^{\text{BE}}(\epsilon) N_{\text{B}} R_{\text{B}}^2}{R_{\text{out}}^2} \right]. \quad (11)$$

The factor 47/4 is a consequence of averaging the inverse square distance within this distribution for the density and the region where the reaction takes place [67]. In Fig. 3 we also show these results (dashed lines), which agree very well with the previous less elaborate model for the distribution of stars. This shows that even if we do not have a quantitative explanation for the anisotropy at the border, different global descriptions of the association point to the same photo-disintegration rate, and the

model we are proposing is stable. It is clear, however, that within the 3 pc HEGRA hot spot the concentration of stars would be above average, and thus hereafter we take as a fiducial value for  $R_A^*$  the one resulting from Eq. (10) (more on this below).

After the high energy nuclei interact with the photon field entering the GDR energy region, the nucleus is left in an excited state which will go over into an excited daughter state emitting  $\gamma$ -rays [54]. Some early semi-quantitative statistical-model calculations for the production of  $\gamma$ -rays through the decay of the GDR in the  $^{56}\text{Fe}$  nucleus showed that the mean energy of the  $\gamma$ -spectrum is  $\overline{E'_{\gamma 56}} \sim 2-4$  MeV and the average multiplicity is  $\overline{n}_{56} \sim 1-3$  [68]. Previous measurements showed that for the case of  $^{16}\text{O}$ , the corresponding values are  $\overline{E'_{\gamma 16}} \sim 5-7$  MeV and  $\overline{n}_{16} \sim 0.3-0.5$  [69]. Hence, in the observer system, these relativistic nuclei are a source of directional  $\gamma$ -rays with energy of the order  $\sim \gamma$  MeV.

### C. TeV Gamma Ray Emission

The low energy cutoff on  $R_A^*$  seen in Fig. 3 will be mirrored in the resulting photon distribution. The  $E^{-2}$  energy behavior of the various nuclear fluxes will not substantially affect this low energy feature. It is a robust consequence of the model, discussed in and below Eq. (18). The energy behavior for photons in the 1–10 TeV region of the HEGRA data is a complex convolution of the energy distributions of the various nuclei participating in the photo-disintegration, with the rate factors appropriate to the eV photon density for the various stellar populations.

Let us define  $dR_A/dE'_\gamma$  as

$$\frac{dR_A}{dE'_\gamma} = \frac{1}{2} \int_0^\infty \frac{n(\epsilon)}{\gamma^2 \epsilon^2} d\epsilon \int_0^{2\gamma\epsilon} \epsilon' \frac{d\sigma_{\gamma A}}{dE'_\gamma}(\epsilon', E'_\gamma) d\epsilon', \quad (12)$$

where  $d\sigma_{\gamma A}(\epsilon', E'_\gamma)/dE'_\gamma$  is the inclusive differential cross section for production of  $\gamma$ -rays from disintegration and  $E'_\gamma$  is the energy of the emitted photon(s) in the rest frame of the nucleus. Assuming the same cosmic ray spectrum as above, the emissivity (number/volume/steradian) of  $\gamma$ -rays coming from nuclei de-excitation can be written as

$$Q_\gamma^{\text{dis}}(E_\gamma) = \sum_A \int \frac{dn_A}{dE_N}(E_N) dE_N \int \frac{dR_A}{dE'_\gamma} \delta[E_\gamma - \gamma E'_\gamma(1 + \cos\theta_\gamma)] dE'_\gamma \frac{d\cos\theta_\gamma}{2}, \quad (13)$$

where  $E_\gamma$  is the energy of the emitted  $\gamma$ -ray in the lab and  $\theta_\gamma$  is the  $\gamma$ -ray angle with respect to the direction of

the excited nucleus. We write the nuclear flux as

$$\sum_A \frac{dn_A}{dE_N}(E_N) = \sum_A N_A \left( \frac{E_N}{E_0} \right)^{-\alpha}, \quad (14)$$

with  $N_A$  a normalization constant, and  $E_0$  set to 1 TeV. Performing the angular integral with the delta-function

constraint leads to

$$Q_\gamma^{\text{dis}}(E_\gamma) = \sum_A \frac{m_N}{2} \int_{\frac{m_N E_\gamma}{2Q}} \frac{dn_A}{dE_N}(E_N) \frac{dE_N}{E_N} \int_{\frac{m_N E_\gamma}{2E_N}}^Q \frac{dR_A}{dE'_\gamma} \frac{dE'_\gamma}{E'_\gamma}, \quad (15)$$

where  $Q$  is the  $Q$ -value of the de-excitation process. If we further approximate the  $\gamma$ -ray spectrum as being monochromatic, with energy equal to its average value ( $\overline{E'_{\gamma A}}$ ), we can write  $d\sigma_{\gamma A}(\epsilon', E'_\gamma)/dE'_\gamma = \overline{n_A} \sigma_A(\epsilon') \delta(E'_\gamma - \overline{E'_{\gamma A}})$ , where  $\overline{n_A}$  is the mean  $\gamma$ -ray multiplicity for a nucleus with atomic number  $A$ . Hence, the emissivity can be approximated by [54]

$$Q_\gamma^{\text{dis}}(E_\gamma) = \sum_A \frac{\overline{n_A} m_N}{2\overline{E'_{\gamma A}}} \int_{\frac{m_N E_\gamma}{2\overline{E'_{\gamma A}}}} \frac{dn_A}{dE_N}(E_N) R_A \frac{dE_N}{E_N}. \quad (16)$$

The  $\gamma$ -ray emissivity is related to the differential flux at the observer's site (assuming there is no absorption) as

$$\frac{dF_\gamma}{dE_\gamma}(E_\gamma) = \frac{V_{\text{dis}}}{4\pi d^2} Q_\gamma^{\text{dis}}(E_\gamma) \quad (17)$$

where  $V_{\text{dis}}$  is the volume of the source (disintegration) region and  $d$  is the distance to the observer.

It is clear from Eq. (16) that if  $R_A^*$  is weakly dependent on  $E_N$  then the observed  $\gamma$ -ray flux will display the same power law behavior as the nuclei population. The HEGRA data show an approximate  $E^{-2}$  behavior for 1 TeV  $\lesssim E_\gamma \lesssim 10$  TeV, corresponding to a boost factor  $10^6 \lesssim \gamma \lesssim 10^7$ . Remarkably, as can be seen in Fig. 3,  $R_A^*$  varies by a factor of only 2 precisely in this region, far less than the 2 orders of magnitude of the primary nucleus flux. In order to evaluate Eq. (16) we approximate the behavior of  $R_A^*$  as roughly constant for  $E_{\text{min}} < E_N < E_{\text{max}}$ , and zero otherwise; where  $E_{\text{min}} \sim 10^6$  GeV and  $E_{\text{max}} \sim 10^7$  GeV. Incorporating Eq. (14) into Eq. (16), we find that for  $\alpha = 2$  and  $E_\gamma < \frac{2\overline{E'_{\gamma A}} E_{\text{min}}}{m_N} \simeq 2$  TeV ( $\overline{E'_{\gamma A}}/1$  MeV)

$$Q_\gamma^{\text{dis}}(E_\gamma) = \sum_A \frac{\overline{n_A} m_N}{4\overline{E'_{\gamma A}}} R_A^* N_A \left( \frac{E_{\text{min}}}{E_0} \right)^{-2}, \quad (18)$$

independent of  $E_\gamma$ , whereas for  $E_\gamma > \frac{2\overline{E'_{\gamma A}} E_{\text{min}}}{m_N} \simeq 2$  TeV ( $\overline{E'_{\gamma A}}/1$  MeV)

$$Q_\gamma^{\text{dis}}(E_\gamma) = \sum_A \frac{\overline{n_A} m_N}{4\overline{E'_{\gamma A}}} R_A^* N_A \left( \frac{E_\gamma}{E_{\gamma 0}} \right)^{-2}, \quad (19)$$

where

$$E_{\gamma 0} = \frac{2\overline{E'_{\gamma A}} E_0}{m_N} \simeq 2000 \overline{E'_{\gamma A}}. \quad (20)$$

The predicted constancy of the flux below  $\sim 2$  TeV implies a strong suppression in this region relative to a flux extrapolated from HEGRA data to maintain an  $E_\gamma^{-2}$  behavior down to lower energies. For example, the upcoming GLAST mission will probe the gamma ray spectrum from the Cygnus region in the range 20 MeV – 300 GeV [70]. The flux predicted at  $\sim 100$  GeV from an  $E_\gamma^{-2}$  extrapolation of the HEGRA data would render the source spectacularly visible in the GLAST observation, whereas the model here would predict a suppression by a factor of  $\sim (2/0.1)^2 = 400$  relative to this extrapolated flux. At 500 GeV the suppression would be still statistically significant:  $E_\gamma^{-2} \times \text{flux}$  falls by a factor of  $\sim 16$ .

The previous discussion has been qualitative. In Fig. 4 these features are displayed following a direct integration of Eq. (16), with choice of parameters to provide eyeball agreement with the data. One can see that the behavior of the fully integrated spectrum agrees in essential characteristics with the results of the preceding qualitative discussion.

All in all, in the present model the photon flux follows the parent population of nuclei in the PeV/nucleon energy region. Consistency then requires the nucleus spectrum not to be significantly steeper than  $E^{-2}$ . How does this comply with experimental data?

As mentioned in Sec. II, the absence of supernova remnants in the association suggests that the nucleus population originates in the diffuse cosmic ray flux rather than in local supernova explosions. In assessing the consistency of the model we first obtain the nuclear population with  $\gamma \sim 10^6$  (i.e., PeV energy/nucleon) necessary for matching the HEGRA data. For simplicity, for this purpose, we approximate the sum in Eq. (16) with a single species (take silicon). Setting the volume  $V = (4/3)\pi r^3$  and the spectral index  $\alpha = 2$ , we find from Eqs. (1) and (17) the normalization constant

$$N_{28} = 1.0 \times 10^{-10} \text{ cm}^{-3} \text{ TeV}^{-1}. \quad (21)$$



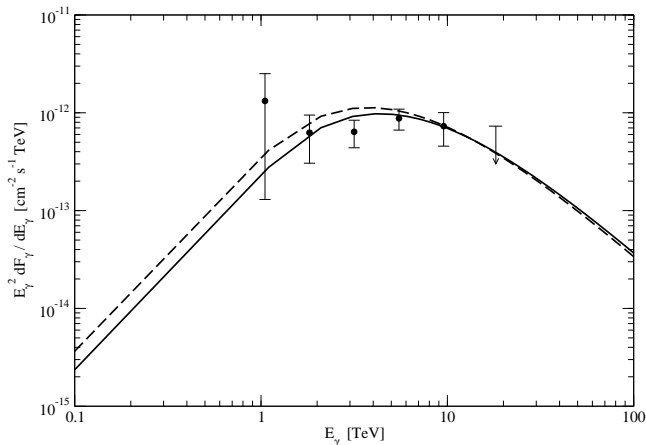


FIG. 4: Energy-weighted  $\gamma$ -ray flux superposed over the HEGRA data. The curves are not actual fits to the spectrum but are based on particular choices of the parameters which provide eyeball agreement with the data. The solid line corresponds to  $^{28}\text{Si}$  and the dashed one to  $^{56}\text{Fe}$ . We have used  $N_{28} = 2 \times 10^{-10} \text{ cm}^{-3} \text{ TeV}^{-1}$  and  $N_{56} = 10^{-10} \text{ cm}^{-3} \text{ TeV}^{-1}$ . In both cases,  $\overline{E}'_{\gamma A} = 1.5 \text{ MeV}$  and the spectral index  $\alpha = 2$ . Note that the choice  $\overline{E}'_{\gamma A} = 1.5 \text{ MeV}$  differs from the value 1 MeV which was used as fiducial input for the discussion in the text.

From Eq. (14) this gives a required Si density at 1 PeV

$$\begin{aligned} \frac{dn_{\text{Si}}}{dE_{\text{Si}}}(E_N = 1 \text{ PeV}) &= \frac{1}{28} \frac{dn_{\text{Si}}}{dE_N}(E_N = 1 \text{ PeV}) \\ &\approx 3.3 \times 10^{-18} \text{ cm}^{-3} \text{ TeV}^{-1} \quad (22) \end{aligned}$$

It is of interest to compare this with the observed diffuse cosmic ray nuclear density  $dn_{\text{CR,Si}}/dE$  in this energy region. From [71], we find

$$\begin{aligned} \frac{dn_{\text{CR,Si}}}{dE}(1 \text{ PeV}) &= \frac{4\pi}{c} J_{\text{CR,Si}}(1 \text{ PeV}) \\ &\approx 1.3 \times 10^{-23} \text{ cm}^{-3} \text{ TeV}^{-1}, \quad (23) \end{aligned}$$

a difference of 5 orders of magnitude. Combined with the observation that the diffuse spectrum has a power index of 3, this shows explicitly that (i) the required population density at PeV/nucleon must arise from acceleration of much more plentiful nuclei that are trapped at much lower energies (ii) the acceleration efficiency of the association must be considerably greater than that

of the Galaxy in order to provide a harder spectrum  $\propto E^{-2}$ . In order to ascertain whether this is possible, we compare the total energy in the nucleus population with the wind energy budget  $\sim 10^{39} \text{ erg/s}$ . Integration of  $E_N dn_{\text{Si}}(E_N)/dE_N$ , with the use of Eq. (21), gives for the volume of the HEGRA source a total energy  $\sim 10^{48} \text{ erg}$  (modulo a logarithmic dependence on the source cutoff). This energy is accumulated over the diffusion time of  $10^4 \text{ yr} = 3 \times 10^{11} \text{ seconds}$ , so that the required power density is 2 orders of magnitude smaller than the kinetic energy budget of the entire association.

In summary, we have presented in detail the criteria for the model to be viable. If future observations should lend credence to the model, significant insights into the acceleration mechanism can be obtained, especially to provide clues with respect to the acceleration efficiency. In completing the explanation of the HEGRA signal, there is of course one issue that needs to be addressed – the signal was observed only in a 3 pc radius cell at the edge of the association. With the same angular radius, there are a total of 37 cells in the core of the association. The flux in each of the other cells is limited to be  $\lesssim 0.17$  of TeV J2032+4130. At this point in our understanding we can provide only qualitative remarks. The obvious possibility is an increased density of very hot OB stars in the cell of TeV J2032+4130 which provide more efficient trapping and accelerating conditions, as well as a hotter photon background. Indeed, a recent estimate [44] indicates around 10 O stars in the region of the source, which is a factor of 3 larger than expected on the basis of a uniform population. (This strongly supports our previous choice of  $R_A^*$ .) More understanding of this can only come with more data and a full Monte Carlo simulation.

#### D. TeV Neutrino Emission

As mentioned above, the interaction of nuclei with the background photons produces a beam of neutrons. The decay mean free path of a neutron is  $c\gamma\bar{\tau}_n = 9.15 (E_n/10^9 \text{ GeV}) \text{ kpc}$ , the lifetime being boosted from its rest-frame value  $\bar{\tau}_n = 886 \text{ seconds}$  to its lab value via  $\gamma = E_n/m_n$ . This means that for a source distance  $d \sim 1.7 \text{ kpc}$ , practically all neutrons with  $E_n \sim 10^6 \text{ GeV}$  will decay *en route* to Earth, producing a flux of directional antineutrinos.

The basic formula that relates the neutron flux at the source ( $dF_n/dE_n$ ) to the antineutrino flux observed at Earth ( $dF_{\bar{\nu}}/dE_{\bar{\nu}}$ ) is [72]

$$\frac{dF_{\bar{\nu}}}{dE_{\bar{\nu}}}(E_{\bar{\nu}}) = \int dE_n \frac{dF_n}{dE_n}(E_n) \left(1 - e^{-\frac{m_n d}{E_n \bar{\tau}_n}}\right) \int_0^{Q_{\bar{\nu}}} d\epsilon_{\bar{\nu}} \frac{dP}{d\epsilon_{\bar{\nu}}}(\epsilon_{\bar{\nu}}) \int_{-1}^1 \frac{d \cos \bar{\theta}_{\bar{\nu}}}{2} \delta [E_{\bar{\nu}} - E_n \epsilon_{\bar{\nu}} (1 + \cos \bar{\theta}_{\bar{\nu}})/m_n]. \quad (24)$$

The variables appearing in Eq. (24) are the antineutrino

and neutron energies in the lab ( $E_{\bar{\nu}}$  and  $E_n$ ), the antineu-

trino angle with respect to the direction of the neutron momentum, in the neutron rest-frame ( $\bar{\theta}_{\bar{\nu}}$ ), and the antineutrino energy in the neutron rest-frame ( $\epsilon_{\bar{\nu}}$ ). The last three variables are not observed by a laboratory neutrino-detector, and so are integrated over. The observable  $E_{\bar{\nu}}$  is held fixed. The delta-function relates the neutrino energy in the lab to the three integration variables. The parameters appearing in Eq. (24) are the neutron mass and rest-frame lifetime ( $m_n$  and  $\bar{\tau}_n$ ). Finally,  $dP/d\epsilon_{\bar{\nu}}$  is the normalized probability that the decaying neutron produces a  $\bar{\nu}$  with energy  $\epsilon_{\bar{\nu}}$  in the neutron rest-frame. Note that the maximum  $\bar{\nu}$  energy in the neutron rest frame is very nearly  $Q_{\bar{\nu}} \equiv m_n - m_p - m_e = 0.78$  MeV. Integration of Eq. (24) can be easily accomplished, especially when two good approximations are applied. In the lab, the ratio of the maximum  $\bar{\nu}$  energy to the neutron energy is  $Q_{\bar{\nu}}/m_n \sim 10^{-3}$ , and so the boosted  $\bar{\nu}$  has a spectrum with  $E_{\bar{\nu}} \in (0, 10^{-3} E_n)$  and an average energy  $\epsilon_0 = 0.48$  MeV. The first approximation is to simplify the antineutrino spectrum from  $\beta$ -decay and take a monochromatic spectrum with energy equal to the average energy,  $\epsilon_0$ . In such a way  $dP/d\epsilon_{\bar{\nu}} = \delta(\epsilon_{\bar{\nu}} - \epsilon_0)$  and Eq. (24) simplifies. The second approximation is to replace the neutron decay probability  $1 - e^{-dm_n/E_n\bar{\tau}_n}$  with a step function  $\Theta(E_n^{\max} - E_n)$  at some energy  $E_n^{\max} \sim \mathcal{O}(m_n d/\bar{\tau}_n) = (d/9.15 \text{ kpc}) \times 10^9 \text{ GeV}$ . Combining these two approximations, one obtains [72]

$$\frac{dF_{\bar{\nu}}}{dE_{\bar{\nu}}}(E_{\bar{\nu}}) = \frac{m_n}{2\epsilon_0} \int_{\frac{m_n E_{\bar{\nu}}}{2\epsilon_0}}^{E_n^{\max}} \frac{dE_n}{E_n} \frac{dF_n}{dE_n}(E_n). \quad (25)$$

The neutron emission can be related to the HEGRA  $\gamma$ -ray flux only if photo-de-excitation following photo-dissociation is unsuppressed. Thus, a *lower* bound for neutron emissivity (and resulting neutrino flux) may be obtained by finding this relation for the cases (Si/Fe) discussed in the previous section. An extremely important example where there is 100% suppression is the case of  ${}^4\text{He}$ , because neutron emission results in transitions to stable  $A = 3$  daughter states [73]. This possibility will be discussed more at the end of this section. Meanwhile, we turn to estimate the neutrino event rate associated with Si dissociation which can be expected at the IceCube detector, now under construction at the South Pole [74].

For a transition in which an average of  $\bar{n}_{28}$   $\gamma$ -rays are emitted during de-excitation, an average of  $\sim 1/2$  neutron is emitted during the stripping (there is almost equal probability of emission of  $n$  and  $p$ ). The conservation of Lorentz factor allows the relation

$$\int^{\gamma \bar{E}'_{\gamma 28}} \frac{dF_{\gamma}}{dE_{\gamma}} dE_{\gamma} = 2 \bar{n}_{28} \int^{\gamma m_n} \frac{dF_n}{dE_n} dE_n. \quad (26)$$

Taking the derivative with respect to  $\bar{\gamma}$  gives the relation

$$\bar{E}'_{\gamma 28} \left. \frac{dF_{\gamma}}{dE_{\gamma}} \right|_{E_{\gamma}=\gamma \bar{E}'_{\gamma 28}} = 2 m_n \bar{n}_{28} \left. \frac{dF_n}{dE_n} \right|_{E_n=\gamma m_n}, \quad (27)$$

which leads to desired relation between photon and neutron fluxes

$$\frac{dF_n}{dE_n}(E_n) = \frac{\bar{E}'_{\gamma 28}}{2m_n \bar{n}_{28}} \frac{dF_{\gamma}}{dE_{\gamma}}(E_{\gamma} = E_n \bar{E}'_{\gamma 28}/m_n). \quad (28)$$

Substituting into Eq. (25), one finds the antineutrino flux associated to a given flux of photons

$$\frac{dF_{\bar{\nu}}}{dE_{\bar{\nu}}}(E_{\bar{\nu}}) = \frac{1}{\alpha} \left( \frac{2\epsilon_0}{\bar{E}'_{\gamma 28}} \right)^{\alpha-1} \frac{1}{2\bar{n}_{28}} \frac{dF_{\gamma}}{dE_{\gamma}}(E_{\gamma} = E_{\bar{\nu}}), \quad (29)$$

where  $\alpha$  is the spectral index of the photon population. When referring to the 3 pc HEGRA cell, and taking  $2\epsilon_0 \simeq \bar{E}'_{\gamma 28}$ , we finally obtain the predicted associated antineutrino flux

$$\frac{dF_{\bar{\nu}}}{dE_{\bar{\nu}}}(E_{\bar{\nu}}) = \frac{1}{4} \frac{N_{\text{HEGRA}}}{\bar{n}_{28}} \left( \frac{E_{\bar{\nu}}}{\text{TeV}} \right)^{-\alpha_{\text{HEGRA}}}. \quad (30)$$

which is valid in the energy window for which nuclei disintegration takes place, i.e.,  $E_{\bar{\nu}} \sim (10^6 - 10^7) \epsilon_0$ .

At IceCube, the events are grouped as either muon tracks or showers. Tracks include muons resulting from both cosmic muons and from Charged Current (CC) interaction of muon neutrinos. The angular resolution for muon tracks  $\approx 0.7^\circ$  [75] allows a search window of  $1^\circ \times 1^\circ$ . This corresponds to a search bin solid angle of  $\Delta\Omega_{1^\circ \times 1^\circ} \approx 3 \times 10^{-4}$  sr. Since IceCube does not resolve the 3 pc HEGRA cell, the  $\bar{\nu}$  flux will have contribution from all 37 cells in the core of the association. To estimate this, we assume that the flux from each of the 36 non-HEGRA cells is equal to the upper limit found in the direction of Cygnus X-3, namely 1/6 of the flux from TeV J2032+4130. The antineutrino flux from the Cygnus region can then be approximated (perhaps generously) as

$$\frac{dF_{\bar{\nu}}}{dE_{\bar{\nu}}}(E_{\bar{\nu}}) = \frac{7}{4} \frac{N_{\text{HEGRA}}}{\bar{n}_{28}} \left( \frac{E_{\bar{\nu}}}{\text{TeV}} \right)^{-\alpha_{\text{HEGRA}}}. \quad (31)$$

To estimate the expected number of  $\bar{\nu}_\mu$  induced tracks from Cygnus OB2 we adopt the semianalytical calculation presented in Ref. [76],

$$\mathcal{N}_{\text{Cyg}}^{\text{tr}} = t n_{\text{T}} \int_{l'_{\min}}^{\infty} dl \int_{m_{\mu}}^{\infty} dE_{\mu}^{\text{fin}} \int_{E_{\mu}^{\text{fin}}}^{\infty} dE_{\mu}^0 \int_{E_{\mu}^0}^{\infty} dE_{\bar{\nu}} \frac{dF_{\bar{\nu}\mu}}{dE_{\bar{\nu}}}(E_{\bar{\nu}}) \frac{d\sigma_{\text{CC}}}{dE_{\mu}^0}(E_{\bar{\nu}}, E_{\mu}^0) F(E_{\mu}^0, E_{\mu}^{\text{fin}}, l) A_{\text{eff}}^0, \quad (32)$$

where  $dF_{\bar{\nu}_\mu}/dE_{\bar{\nu}}$  is the  $\bar{\nu}_\mu$  flux,  $d\sigma_{CC}/E_\mu^0$  is the differential CC interaction cross section producing a muon of energy  $E_\mu^0$ ,  $n_T$  is the number density of nucleons in the matter surrounding the detector, and  $t$  is the exposure time of the detector. After being produced, the muon propagates through the rock and ice surrounding the detector and loses energy. We denote by  $F(E_\mu^0, E_\mu^{\text{fin}}, l)$  the function that represents the probability of a muon produced with energy  $E_\mu^0$ , arriving at the detector with energy  $E_\mu^{\text{fin}}$ , after traveling a distance  $l$ . The details of the detector are encoded in the effective area  $A_{\text{eff}}^0$ . We use the parametrization of the  $A_{\text{eff}}^0$  described in Ref. [76] to simulate the response of the IceCube detector after events that are not neutrinos have been rejected (this is achieved by quality cuts referred to as “level 2” cuts in Ref. [74]). The minimum track length cut is  $l_{\text{min}} = 300$  m and we account for events with  $E_\mu^{\text{fin}} > 500$  GeV.

Although the flux of antineutrinos produced by Cygnus OB2 is pure  $\bar{\nu}_e$ , because of neutrino oscillations, the antineutrinos observed at Earth will be distributed over all flavors,

$$\frac{dF_{\bar{\nu}_\alpha}}{dE_{\bar{\nu}}} = \left( \frac{1}{3} + f_{\bar{\nu}_e \rightarrow \bar{\nu}_\alpha}(E_{\bar{\nu}}) \right) \frac{dF_{\bar{\nu}}}{dE_{\bar{\nu}}}, \quad (33)$$

where  $\alpha = e, \mu, \tau$  denotes the neutrino flavor. The 95% confidence ranges for the probability differences,

$$\begin{aligned} f_{\bar{\nu}_e \rightarrow \bar{\nu}_\mu} &= -0.106_{-0.082}^{+0.060}, \\ f_{\bar{\nu}_e \rightarrow \bar{\nu}_\tau} &= -0.128_{-0.055}^{+0.089}, \\ f_{\bar{\nu}_e \rightarrow \bar{\nu}_e} &= -(f_{\bar{\nu}_e \rightarrow \bar{\nu}_\mu} + f_{\bar{\nu}_e \rightarrow \bar{\nu}_\tau}), \end{aligned} \quad (34)$$

were derived elsewhere [77] using the results of the up-to-date  $3\nu$  oscillation analysis of solar, atmospheric, LBL and reactor data [78]. Substituting Eqs. (33) and (34) into Eq. (32) we obtain the  $\bar{\nu}_\mu$ -induced tracks in IceCube from Cygnus OB2 in  $t = 15$  years of observation,  $\mathcal{N}_{\text{Cyg}}^{\text{tr}} \approx 7.5/\overline{n_{28}}$ .

Showers are generated by neutrino collisions —  $\nu_e$  or  $\nu_\tau$  CC interactions, and all Neutral Current (NC) interactions — inside of or nearby the detector, and by muon bremsstrahlung radiation near the detector. For showers, the angular resolution is significantly worse than for muon tracks. In our analysis, we consider a shower search bin solid angle,  $\Delta\Omega_{10^\circ \times 10^\circ}$ . Normally, a reduction of the muon bremsstrahlung background is effected by placing a cut of 40 TeV on the minimum reconstructed energy [79]. For Cygnus OB2, this strong energy cut is not needed since this muon background is filtered by the Earth. Thus we account for all events with shower energy  $E_{\text{sh}} \geq E_{\text{sh}}^{\text{min}} = 1$  TeV. The directionality requirement, however, implies that the effective volume for detection of showers is reduced to the instrumented volume of the detector,  $\mathcal{V}_{\text{eff}} = 1 \text{ km}^3$ , because of the small size of the showers (less than 200 m in radius) in this energy range. Following Ref. [77] we estimate the expected number of showers from Cygnus OB2 as

$$\mathcal{N}_{\text{Cyg}}^{\text{sh}} = \mathcal{N}_{\text{Cyg}}^{\text{sh,CC}} + \mathcal{N}_{\text{Cyg}}^{\text{sh,NC}}, \quad (35)$$

where

$$\mathcal{N}_{\text{Cyg}}^{\text{sh,CC}} = t n_T \mathcal{V}_{\text{eff}} \int_{E_{\text{sh}}^{\text{min}}}^{\infty} dE_{\bar{\nu}} \sum_{\alpha=e,\tau} \frac{dF_{\bar{\nu}_\alpha}}{dE_{\bar{\nu}}}(E_{\bar{\nu}}) \sigma_{CC}(E_{\bar{\nu}}), \quad (36)$$

and

$$\mathcal{N}_{\text{Cyg}}^{\text{sh,NC}} = t n_T \mathcal{V}_{\text{eff}} \int_{E_{\bar{\nu}} - E_{\text{sh}}^{\text{min}}}^{\infty} dE_{\bar{\nu}}' \int_{E_{\text{sh}}^{\text{min}}}^{\infty} dE_{\bar{\nu}} \sum_{\alpha=e,\mu,\tau} \frac{dF_{\bar{\nu}_\alpha}}{dE_{\bar{\nu}}}(E_{\bar{\nu}}) \frac{d\sigma_{\text{NC}}}{dE_{\bar{\nu}}'}(E_{\bar{\nu}}, E_{\bar{\nu}}'). \quad (37)$$

Here,  $d\sigma_{\text{NC}}/dE_{\bar{\nu}}'$  is the differential NC interaction cross section producing a secondary antineutrino of energy,  $E_{\bar{\nu}}'$ . In writing Eqs. (36) and (37) we are assuming that for contained events the shower energy corresponds with the interacting  $\bar{\nu}_e$  or  $\bar{\nu}_\tau$  antineutrino energy ( $E_{\text{sh}} = E_{\bar{\nu}}$ ) in a CC interaction, while for NC the shower energy corresponds to the energy in the hadronic shower  $E_{\text{sh}} = E_{\bar{\nu}} - E_{\bar{\nu}}' \equiv y E_{\bar{\nu}}$  where  $y$  is the usual inelasticity parameter in deep inelastic scattering. In total we expect  $\mathcal{N}_{\text{Cyg}}^{\text{sh}} \approx 5/\overline{n_{28}}$  from Cygnus OB in 15 years of observation.

We now turn to the estimate of the background of

atmospheric neutrinos. For the “conventional” atmospheric neutrino fluxes arising from pion and kaon decays, we adopt the 3-dimensional scheme estimates of Ref. [80], which we extrapolate to match at higher energies the 1-dimensional calculations by Volkova [81]. We also incorporate “prompt” neutrinos from charm decay as calculated in Ref. [82]. We obtain the number of expected track and shower events from atmospheric neutrinos as in Eqs (32), (36), and (37) with  $dF_{\nu_\alpha}^{\text{ATM}}/dE_\nu(E_\nu)$  being the  $\nu_e$  and  $\nu_\mu$  atmospheric neutrino fluxes integrated over a solid angle of  $1^\circ \times 1^\circ$  (for tracks) and  $10^\circ \times 10^\circ$  (for showers) width around the direction of the Cygnus OB2

Primary quanta	$\gamma$ production mech.	$\nu$ production mech.	Number ratio	Energy ratio	comments
A	$A \rightarrow A^* \rightarrow \sim \overline{n_A} \gamma + A$ [ $E_\gamma \sim \gamma_A \overline{E}'_{\gamma A}$ ]	$A \rightarrow n \rightarrow \overline{\nu}_e$ [ $E_\nu \sim \gamma_A \epsilon_0$ ]	$\gamma : \nu \sim \overline{n_A} : 1/2$	$\frac{E_\gamma}{E_\nu} \sim \frac{E'_{\gamma A}}{\epsilon_0}$ $\sim 2 - 8$	observation of $\nu$ 's at IceCube depends on ${}^4\text{He}$ abundance
p	$p \rightarrow \pi^0 \rightarrow 2 \gamma$ [ $E_\gamma \sim \frac{1}{10} E_p$ ]	$p \rightarrow \pi^\pm \rightarrow 3 \nu$ [ $E_\nu \sim \frac{1}{20} E_p$ ]	$\gamma : \nu \sim 1 : 3$	$\frac{E_\gamma}{E_\nu} \sim 2$	$\nu$ 's ARE seen at IceCube
e-plasma	synchrotron inverse Compton	none			

TABLE I: Comparison of  $\gamma$ -ray and neutrino emission from  $A$ ,  $p$ , and  $e$  primaries. Note that per  $\gamma$ -ray, an order of magnitude fewer neutrinos are expected from nuclei photodisintegration than from hadronic interactions followed by pion decays. Note also that the neutrino energy from the nuclei photo-disintegration is typically about one order of magnitude smaller than the  $\gamma$ -ray energy. When the primaries are electrons, only  $\gamma$ -rays are produced, but not neutrinos.

source  $\theta = 131.2^\circ$ . We get an expected background of  $\mathcal{N}_{\text{ATM}}^{\text{tr}} = 14$  and  $\mathcal{N}_{\text{ATM}}^{\text{sh}} = 47$  in 15 years. Of the 47 showers, 16 correspond to  $\nu_e$  CC interactions while 31 correspond to  $\nu_\mu$  NC interactions.

It is clear from the preceding that there is no significant antineutrino signal resulting from dissociations which are accompanied by unsuppressed photo-de-excitation. This is in complete contrast with the  $pp$  case where for an spectral index of 2 one expects on average a flux of  $\nu_\mu$  half of that of  $\gamma$ -rays [83, 84, 85, 86, 87] (see Sec. V). Then, when considering the 37 cells of the Cygnus OB2 association one expects a  $\nu_\mu$  event rate of  $4.2 \text{ yr}^{-1}$  with a background of  $0.9 \text{ yr}^{-1}$ . The track signal in the  $pp$  case is about an order of magnitude larger than in the  $A^*$  case. Because of production and oscillations the  $pp$  mechanism yields about one  $\nu_\mu$  per  $\gamma$ -ray. The yield in the  $A^*$  mechanism (for  $\overline{n_{28}} = 2$ ) is about 0.25  $\overline{\nu}_e$  per  $\gamma$ -ray which, after oscillation, yields 0.05  $\overline{\nu}_\mu$  per  $\gamma$ -ray. This ratio decreases by an additional factor of  $\sim 2$  if comparison is made with integrated spectrum above 1 TeV.

We turn now to comment on the role of helium. Except for protons, helium nuclei dominate the cosmic ray spectrum, with a population about 100 times larger than the heavy species [88, 89]. As mentioned above, the stripping of a nucleon from  ${}^4\text{He}$  leaves the residual  $A = 3$  nuclides in their ground states [73], so that there is no photon emission. However, stripping to  ${}^3\text{He}$  with emission of a neutron will provide a yield of neutrinos. As can be seen from Fig. 3, the stripping rate is down by an order of magnitude from that for the heavy elements so that, with the larger population, the expected antineutrino flux would be about a factor of 10 larger than our prediction from Eq. (31). This enhancement has powerful consequences for the source energetics: the energy required to accelerate the entire  ${}^4\text{He}$  population is very close to the allowed energy budget for the diffusion lifetime. Therefore, should IceCube obtain a statistically significant signal that cannot be ascribed to  $pp$  interaction (because of observation of the TeV  $\gamma$ -ray suppression predicted by the model), then there could be a hint of extraordinary efficiency in the trapping an accelerating mechanisms in extremely hot and intense stellar associa-

tions.

## V. PHOTO-DISINTEGRATION vs $\pi$ DECAY

In the previous section we have described the mechanism of  $\gamma$ -ray production from nuclei de-excitation after disintegration in the background photon field and showed that the HEGRA data could be explained in these terms. In addition, this mechanism can give rise to a neutrino flux after the stripped neutrons decay in flight. However, as we mentioned in the Introduction, there are two channels other than photo-disintegration that might contribute to  $\gamma$ -ray and neutrino production at the Cygnus region. These are photo-hadronic ( $A$ - $\gamma$ ) and pure hadronic ( $A$ - $p$ ) interactions. In both cases,  $\gamma$ -rays (neutrinos) are produced after  $\pi^0$  ( $\pi^+$  and  $\pi^-$ ) decays.

As noted above, photo-meson production has a very high energy threshold, being only relevant for very high energetic beams or in very hot photon environments. Even in these extreme cases, the fact that this reaction turns on at so high energies implies that the photons and neutrinos from decaying pions are produced at very high energies too, well above the TeV range. Hence, in the following subsections we comment on the  $\gamma$ -ray and neutrino emissivities due to nucleus-proton collisions and compare it with those calculated for the photo-disintegration of nuclei. But first, in Table I we show approximate estimates for the energy, number ratio and energy ratio of neutrinos and  $\gamma$ -rays due to photo-disintegration and pion decay at production (we have also included the leptonic mechanism of  $\gamma$ -ray production for completeness). Now, we will compare these two hadronic mechanisms.

### A. $\pi$ spectrum

The interaction of high energy nuclei with the cold ambient interstellar medium (ISM) gives rise to  $\gamma$ -rays through the decay of the produced neutral mesons. The  $\pi^0$  emissivity resulting from an isotropic distribution of

accelerated nuclei  $dn(E_N)/dE_N$  is given by [90]

$$Q_{\pi^0}^{Ap}(E_{\pi^0}) = c n_H \int_{E_N^{th}(E_{\pi^0})}^{E_N^{max}} \frac{dn}{dE_N}(E_N) \times \frac{d\sigma_A}{dE_{\pi^0}}(E_{\pi^0}, E_N) dE_N \quad (38)$$

where  $n_H$  is the ISM number density,  $E_N^{th}(E_{\pi^0})$  is the minimum energy per nucleon required to produced a pion with energy  $E_{\pi^0}$ , and  $d\sigma_A(E_{\pi^0}, E_N)/dE_{\pi^0}$  is the differential cross section for the production of a pion with energy  $E_{\pi^0}$  in the lab frame due to the collision of a nuclei  $A$  of energy per nucleon  $E_N$  with a hydrogen atom at rest.

Hence, an accurate knowledge of the differential cross section for pion production is necessary to calculate the  $\gamma$ -ray emissivity from this channel. There have been several approaches and parameterizations in the literature, most of them based on the use of the isobaric [91] and scaling [92, 93] models of the reaction or their combination [94, 95, 96]. The  $\delta$ -function approximation was

considered in Ref. [97] and the inclusion of diffractive interactions and scaling violations in Ref. [98] (see the Appendix of Ref. [99] for a comparison of different approaches). A new recent parameterization is presented in Ref. [100] based on simulations of proton-proton interactions from the SIBYLL event generator [101]. The isobaric model has been shown to work reasonably well at low energies ( $E < 3$  GeV), whereas the scaling model is more suitable at higher energies. Hence, here we will follow the scaling model with a parameterization of the differential cross section which is an  $E_N$ -independent approximation of that given in Ref. [100]

$$\frac{d\sigma_A}{dE_{\pi^0}}(E_{\pi^0}, E_N) \simeq \frac{\sigma_0^A}{E_{\pi^0}} f_{\pi^0}(x) \quad (39)$$

where  $x \equiv E_{\pi^0}/E_N$  and  $\sigma_0^A = A^{3/4} \sigma_0$ , with  $\sigma_0 = 34.6$  mb, which takes into account the scaling of the cross section with the atomic number [102], and

$$f_{\pi^0}(x) \simeq 8.18 x^{1/2} \left( \frac{1 - x^{1/2}}{1 + 1.33 x^{1/2} (1 - x^{1/2})} \right)^4 \left( \frac{1}{1 - x^{1/2}} + \frac{1.33 (1 - 2x^{1/2})}{1 + 1.33 x^{1/2} (1 - x^{1/2})} \right) \quad (40)$$

which takes into account the high pion multiplicities at high energies.

By using this form for the differential cross section and a power-law cosmic-ray spectrum, the  $\pi^0$  emissivity can be written as

$$Q_{\pi^0}^{Ap}(E_{\pi^0}) \simeq Z_{A\pi^0}(\alpha) Q_A^{Ap}(E_{\pi^0}^0) \quad (41)$$

where

$$Q_A^{Ap}(E_N) = \sigma_0^A c n_H \frac{dn}{dE_N}(E_N) \quad (42)$$

and the spectrum-weighted moment of the inclusive cross section or so-called  $Z$ -factor is given by

$$Z_{A\pi^0}(\alpha) \equiv \int_0^1 x^{\alpha-2} f_{\pi^0}(x) dx \quad (43)$$

where, as usual,  $\alpha$  is the spectral index of the cosmic-ray spectrum.

## B. TeV $\gamma$ -rays

Since isotropy is implied in Eq. (38), the  $\gamma$ -ray emissivity is obtained from the  $\pi^0$  emissivity as

$$Q_{\gamma}^{Ap}(E_{\gamma}) = 2 \int_{E_{\pi^0}^{\min}(E_{\gamma})}^{E_{\pi^0}^{\max}(E_{\pi^0})} \frac{Q_{\pi^0}^{Ap}(E_{\pi^0})}{(E_{\pi^0}^2 - m_{\pi^0}^2)^{1/2}} dE_{\pi^0} \quad (44)$$

where  $E_{\pi^0}^{\min}(E_{\gamma}) = E_{\gamma} + m_{\pi^0}^2/(4E_{\gamma})$ . Hence, the  $\gamma$ -ray emissivity is given by

$$Q_{\gamma}^{Ap}(E_{\gamma}) \simeq Z_{\pi^0\gamma}(\alpha) Q_{\pi^0}^{Ap}(E_{\gamma}) \quad (45)$$

with  $Z_{\pi^0\gamma}(\alpha) = 2/\alpha$ .

On the other hand, the  $\gamma$ -ray emissivity due to nuclei photo-disintegration, Eq. (16), in the range of energies where  $R_A$  is approximately constant, can be written as

$$Q_{\gamma}^{\text{dis}}(E_{\gamma}) \simeq Z_{A\gamma}(\alpha) Q_A^{\text{dis}}(E_{\gamma}) \quad (46)$$

where, assuming dominance of a single component (silicon),

$$Z_{A\gamma}(\alpha) = \left( \frac{\overline{n}_{28}}{\alpha} \right) \left( \frac{2\overline{E}'_{\gamma 28}}{m_N} \right)^{\alpha-1} \quad (47)$$

$$Q_A^{\text{dis}}(E_N) = R_A \frac{dn}{dE_N}(E_N) \quad (48)$$

Hence, the ratio of the  $\gamma$ -ray emissivity due to these two mechanisms is given by,

$$R_{Ap/dis}^\gamma(\alpha) \equiv \frac{Q_\gamma^{Ap}(E_\gamma)}{Q_\gamma^{dis}(E_\gamma)} \simeq 0.1 \left( \frac{n_H}{0.1 \text{ cm}^{-3}} \right) \left( \frac{A}{28} \right)^{3/4} \left( \frac{10^{-5} \text{ yrs}^{-1}}{R_A} \right) \left( \frac{0.005}{Z_{A\gamma}(\alpha)} \right) \left( \frac{Z_{A\pi^0}(\alpha) Z_{\pi^0\gamma}(\alpha)}{Z_{A\pi^0}(2) Z_{\pi^0\gamma}(2)} \right) \quad (49)$$

Thus, for  $n_H = 0.1 \text{ cm}^{-3}$  as quoted in the model of Ref. [48],  $\gamma$ -rays from nuclei dissociation dominate those from pion decays produced in hadronic interactions by as much as an order of magnitude. Note however that in the model of Ref. [48] the volume-integrated luminosity  $\int Q_\gamma^{Ap}(E_\gamma) dV \propto n_H^{-1/2}$ . Thus, within this model, a higher density would *decrease* the hadronic  $\gamma$ -ray flux coming from this region. As suggested in Ref. [48], we have taken  $n_H = 0.1 \text{ cm}^{-3}$  which, for the concentration of stars in the Cygnus OB2 region, corresponds to a volume of interaction equal to that of the region of the HEGRA signal.

Hence,  $\gamma$ -rays produced by the de-excitation of nuclei after photo-dissociation in the photon background might well be the primary contribution to the TeV signal from the Cygnus OB2 region.

### C. TeV neutrinos

The interaction of high energy nuclei with protons of the ISM gives rise to a neutrino (and antineutrino) emissivity at production which, in an analogous manner as in the previous case, can be expressed as

$$Q_{\nu_\mu}^{Ap}(E_{\nu_\mu}) = 2 [Z_{\pi^0\nu_\mu}(\alpha) + Z_{\mu\nu_\mu}(\alpha)] Q_{\pi^0}^{Ap}(E_{\nu_\mu}) \quad (50)$$

$$Q_{\nu_e}^{Ap}(E_{\nu_e}) = 2 Z_{\mu\nu_e}(\alpha) Q_{\pi^0}^{Ap}(E_{\nu_e}) \quad (51)$$

where the factor 2 takes into account the sum of both neutrino and antineutrino emissivities, and  $Z_{\pi^0\nu_\mu}(\alpha)$ ,  $Z_{\mu\nu_\mu}(\alpha)$  and  $Z_{\mu\nu_e}(\alpha)$  are the  $Z$ -factors corresponding to  $\nu_\mu$  from pion and muon decay and  $\nu_e$  from muon decay, respectively. They are given by [100]

$$Z_{\pi^0\nu_\mu}(\alpha) = \frac{(1-r)^{\alpha-1}}{\alpha} \quad (52)$$

$$Z_{\mu\nu_\mu}(\alpha) = \frac{4 [3 - 2r - r^\alpha (3 - 2r + \alpha - \alpha r)]}{\alpha^2 (1-r)^2 (\alpha+2) (\alpha+3)} \quad (53)$$

$$Z_{\mu\nu_e}(\alpha) = \frac{24 [\alpha(1-r) - r(1-r^\alpha)]}{\alpha^2 (1-r)^2 (\alpha+1) (\alpha+2) (\alpha+3)} \quad (54)$$

where  $r = (m_\mu/m_\pi)^2 = 0.467$ . Hence, after taking into account oscillations, the ratio of muon and electron neutrinos plus antineutrinos to  $\gamma$ -rays of the same energy for  $\alpha \in (1.5, 3)$  is approximately given by (and in good agreement with Refs. [83, 84, 85, 86, 87])

$$R_{\nu_\mu/\gamma}^{Ap}(\alpha) \sim 1.05 - 0.28 \alpha \quad (55)$$

$$R_{\nu_e/\gamma}^{Ap}(\alpha) \sim 1.08 - 0.28 \alpha \quad (56)$$

Thus, the predicted ratios for  $\nu_e:\nu_\mu:\nu_\tau:\gamma$  at a common energy are  $\sim 1:1:1:1$ ; here we have included  $\nu_\mu-\nu_\tau$  equilibration which gives the added information that  $\nu_\tau:\nu_\mu=1:1$ .

Note that at the high energies we are interested in, the ratio of the number of neutrinos to that of  $\gamma$ -rays at the same energy, is smaller than the expected 3:1. The reason being that the average neutrino energy is about a quarter of that of the parent pion, while in the case of the photon it is half. Hence there are more very low energy neutrinos than very low energy photons, which compensates what happens at higher energies, so that the ratio of the *total* number of neutrinos to that of photons is indeed 3:1.

On the other hand, for the nuclei disintegration case, from Eq. (29), the neutrino emissivity at production can be written as

$$Q_{\bar{\nu}_e}^{dis}(E_{\bar{\nu}_e}) = R_{n/\gamma}^{dis}(\alpha) Z_{n\nu}(\alpha) Q_\gamma^{dis}(E_{\bar{\nu}_e}) \quad (57)$$

where the  $Z$ -factor associated to the antineutrino emission from neutron decay and the ratio of neutrons to  $\gamma$ -rays of the same energy,  $R_{n/\gamma}^{dis}$ , are given by

$$Z_{n\nu}(\alpha) = \left( \frac{1}{\alpha} \right) \left( \frac{2\epsilon_0}{m_N} \right)^{\alpha-1} \quad (58)$$

$$R_{n/\gamma}^{dis}(\alpha) = \frac{1}{2\bar{n}_{28}} \left( \frac{m_N}{E'_{\gamma 28}} \right)^{\alpha-1} \quad (59)$$

Hence, the ratios of neutrinos (after taken into account oscillations) due to the  $Ap$  and photo-dissociation mechanisms are given by

$$\begin{aligned}
R_{Ap/dis}^{\nu\mu}(\alpha) &\simeq 4.2 \left( \frac{n_H}{0.1 \text{ cm}^{-3}} \right) \left( \frac{A}{28} \right)^{3/4} \left( \frac{10^{-5} \text{ yrs}^{-1}}{R_A} \right) \\
&\times \left( \frac{R_{\nu\mu/\gamma}^{Ap}(\alpha)}{R_{\nu\mu/\gamma}^{Ap}(2)} \right) \left( \frac{R_{n/\gamma}^{dis}(2) Z_{n\nu}(2) Z_{A\gamma}(2)}{R_{n/\gamma}^{dis}(\alpha) Z_{n\nu}(\alpha) Z_{A\gamma}(\alpha)} \right) \left( \frac{Z_{A\pi^0}(\alpha) Z_{\pi^0\gamma}(\alpha)}{Z_{A\pi^0}(2) Z_{\pi^0\gamma}(2)} \right)
\end{aligned} \tag{60}$$

$$\begin{aligned}
R_{Ap/dis}^{\nu e}(\alpha) &\simeq 1.8 \left( \frac{n_H}{0.1 \text{ cm}^{-3}} \right) \left( \frac{A}{28} \right)^{3/4} \left( \frac{10^{-5} \text{ yrs}^{-1}}{R_A} \right) \\
&\times \left( \frac{R_{\nu e/\gamma}^{Ap}(\alpha)}{R_{\nu e/\gamma}^{Ap}(2)} \right) \left( \frac{R_{n/\gamma}^{dis}(2) Z_{n\nu}(2) Z_{A\gamma}(2)}{R_{n/\gamma}^{dis}(\alpha) Z_{n\nu}(\alpha) Z_{A\gamma}(\alpha)} \right) \left( \frac{Z_{A\pi^0}(\alpha) Z_{\pi^0\gamma}(\alpha)}{Z_{A\pi^0}(2) Z_{\pi^0\gamma}(2)} \right)
\end{aligned} \tag{61}$$

i.e.,  $\nu_\mu$  (and  $\nu_\tau$ ) is suppressed by the factor 4.2 in photo-dissociation relative to  $Ap$ , and  $\nu_e$  is suppressed by 1.8. We note that the neutrino flavor results here agree with the well-known neutrino flavor ratios  $\sim 5:2:2$  and  $\sim 1:1:1$  from astrophysical neutron and pion decay.

Therefore, if the TeV  $\gamma$ -ray signal from the Cygnus OB2 region can be explained by de-excitation of daughter nuclei after photo-dissociation, the neutrino population will be, in general, dominated by pion decay. However, with a significant population of  ${}^4\text{He}$ , this may not be the case: through photo-dissociation  ${}^4\text{He}$  only contributes to the  $\bar{\nu}_e$ -flux without affecting the photon signal. Photon production from  ${}^4\text{He}$   $p$  interactions are negligible, see Eq. (49).

## VI. EeV COSMIC RAY EXCESS?

A seemingly different, but in fact closely related subject we will discuss in this section is the intriguing anisotropy that has been observed by several experiments in the energy range near  $10^9$  GeV  $\equiv$  EeV. Analyses of the data collected by the Akeno Giant Air Shower Array (AGASA) seem to indicate a  $4\sigma$  excess of events from the direction of the Galactic plane in the narrow energy window  $10^{8.9}$  GeV to  $10^{9.5}$  GeV [103]. A Galactic plane enhancement at the  $3.2\sigma$  level between  $10^{8.3}$  GeV and  $10^{9.5}$  GeV has also been reported by the Fly's Eye Collaboration [104]. The anisotropy in the AGASA data sample is dominated by hot spots near the Galactic center and the Cygnus region. However, based on a data sample larger than any previous experiment, the Pierre Auger Collaboration has reported no evidence for such an excess from the direction of the Galactic center [105].

The complete isotropy below about  $10^{7.7}$  GeV revealed by KASCADE data [106] vitiates direction-preserving photons as primaries. Therefore, the excess from the Galactic plane is very suggestive of neutrons as candidate primaries, because the directional signal requires relatively-stable neutral primaries, and time-dilated neutrons can reach the Earth from typical Galactic distances

when the neutron energy exceeds  $10^9$  GeV. The analysis of Fly's Eye data [104] implies that if neutrons are the carriers of the anisotropy, there *needs to be* some contribution from at least one source closer than  $\sim 2$  kpc. As we mentioned in the Introduction, the full Fly's Eye data include a directional signal from the Cygnus region which was somewhat lost in an unsuccessful attempt [12] to relate it to  $\gamma$ -ray emission from Cygnus X-3. This signal was also observed with the Akeno air shower array (see Fig. 1) [13]. As shown in Fig. 2, Cygnus OB2 overlaps along our line of sight with Cygnus X-3, which lies about 8 kpc farther away than the stellar association.

In the context of Cygnus X-3, we note that the 1989 analysis [107] of data collected in the Haverah Park experiment was consistent with the absence of anisotropy in the direction of that source, in the energy bin of interest. There was indeed an excess, with a Poissonian probability of 0.013, but at energies above  $10^{9.6}$  GeV. However, a more recent analysis by the group at Leeds [108], based on improved shower simulations, more selective trigger criteria, and a reduction of the zenith acceptance from  $60^\circ$  to  $45^\circ$ , reveals that previous [109] energy estimates need to be reduced by about 30%. It is then suggestive that the excess may overlap the region of interest. One can encourage an event-by-event analysis to see whether this is indeed the case; in the meantime one may reserve judgment with respect to presence or absence of anisotropy in the Haverah Park data.

More recently, the HiRes Collaboration has carried out a systematic search for point sources in the Northern sky. In an initial series of papers, they report no significant excess for energies greater than  $10^{9.5}$  GeV [110],  $10^{10}$  GeV [111], and  $10^{10.6}$  GeV [112]. All these energy thresholds exceed the range above  $10^{8.7}$  GeV where the Akeno and Fly's Eye anisotropies were reported. Motivated by the present study, we have asked the HiRes Collaboration to extend their analysis down to the energy threshold of interest, in the direction of Cygnus. The result is that there is no significant excess above background for the same angular and energy cuts used by Akeno and Fly's Eye, this with a larger data sample

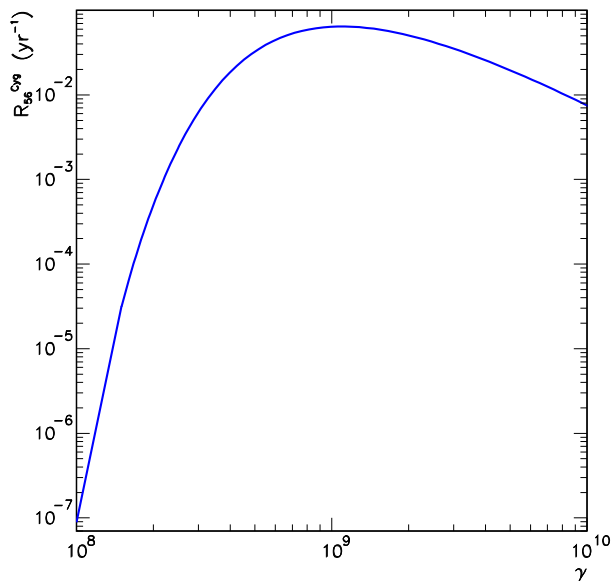


FIG. 5: Photo-disintegration rate of  $^{56}\text{Fe}$  on the  $T = 50$  K Cygnus OB2 blackbody radiation as given by Eq. (8).

than available to either of these previous studies [113]. Additional scans were performed for nearby energy and angular cuts, with the same result of no significant excess. If the previously-reported anisotropies were not statistical fluctuations, then they can be associated with bursts over periods of less than 15 years. This possibility can be monitored with data to be collected at the Northern site of the Pierre Auger Observatory [114].

In what follows, we will proceed on the assumption that the anisotropy reported by the Fly’s Eye [12] and Akeno [13] collaborations originated in a burst taking place in Cygnus OB2 during a 10-yr period, and assess the implications for source energetics.

For nuclei with energies EeV/nucleon, the dissociation proceeds via collisions with far infrared thermal photons populating molecular clouds with temperature  $\sim 50$  K [115]. The photo-disintegration rate is shown in Fig. 5, giving an interaction time of about 100 yr, which allows a perturbative treatment during a 10 yr burst. We can then use Eq. (9) with the left hand side set equal to the neutron luminosity for energies above  $E_1 = 0.5$  EeV. Specifically,

$$\begin{aligned} \frac{dN}{dt} &= 4\pi d^2 e^{d/4.6 \text{ kpc}} \int_{E_1}^{\infty} \left. \frac{dF_n}{dE_n} \right|_{\oplus} dE_n \\ &\approx 7 \times 10^{27} \text{ neutrons s}^{-1}, \end{aligned} \quad (62)$$

where

$$\int_{E_1}^{\infty} \left. \frac{dF_n}{dE_n} \right|_{\oplus} dE_n \simeq 2 \times 10^{-17} \text{ cm}^{-2} \text{ s}^{-1} \quad (63)$$

is the flux observed at Earth [12, 13], and the factor  $e^{d/4.6 \text{ kpc}}$  corrects for neutron  $\beta$ -decay. Now, taking  $R_{56}^{\text{Cyg}} \approx 10^{-2} \text{ yr}^{-1}$  we obtain

$$\int_{E_1} \frac{dn_{\text{Fe}}}{dE_N} dE_N = 5.6 \times 10^{-30} \text{ cm}^{-3}. \quad (64)$$

Assuming a nucleus power law spectrum  $dF_{\text{Fe}}/dE = N_{56} E^{-2}$ , Eq. (64) will determine the normalization constant. Then, the energy density can be obtained via

$$\mathcal{E} = \int_{E_1} E \frac{dn_{\text{Fe}}}{dE} dE, \quad (65)$$

and so straightforward calculation shows that the total energy  $4\pi R^3 \mathcal{E}/3 = 5 \times 10^{35}$  erg is well within the kinetic energy budget of a 10 yr burst.

## VII. CONCLUSIONS

Over the last few decades, the Cygnus region has been the focus of extensive study with a view to understanding astrophysical phenomena in very energetic environments. Interesting observations have been made, but have not held up at statistically significant levels. More recently, improved efficiency and higher resolution have provided signals at discovery level. Perhaps, the most precise of such signals is the (1999-2002) HEGRA detection of the unidentified TeV J2032+4130 source, with an average flux  $\sim 3\%$  of the Crab Nebula [15]. This bright “hot spot”, at the edge of the very active Cygnus OB2 star association, has been recently confirmed through a re-analysis of “old” data collected with the Whipple Observatory [16]. However, the average flux ( $\sim 12\%$  of the Crab) detected during 1989-1990 is well above that reported by the HEGRA Collaboration. Neither the Whipple nor the HEGRA experiments see any evidence for variability within their individual databases. The large differences between the flux levels cannot be explained as errors in estimation of the sensitivity of the experiments because they have been calibrated by the simultaneous observations of other TeV sources. Certainly more data are needed to resolve this issue. Happily, data are currently flowing from the Milagro telescope [116] and the Tibet Air Shower Array [117] experiments at a significant rapid rate.

In this paper, we have focussed on the unidentified TeV  $\gamma$ -ray source observed by the HEGRA Collaboration. Because of the absence of X-ray or radio counterparts, it has been difficult to provide a compelling explanation for the origin of the  $\gamma$ -rays from the HEGRA source. This has motivated us to present an alternative model, which has some well-defined predictions for future observations, both in  $\gamma$ -ray facilities and at neutrino telescopes such as IceCube. The model proposes that the observed TeV  $\gamma$ -rays are the result of Lorentz-boosted MeV  $\gamma$ -rays emitted on the de-excitation of daughter nuclei following collisions of PeV nuclei with a hot ultraviolet photon background. Our results include the following:



(1) There is a specific prediction of a suppression on the  $\gamma$ -ray spectrum in the region  $\lesssim 1$  TeV – this because of the need to achieve the Giant Dipole Resonance for disintegration through collision with  $\sim$  few eV photons.

(2) The flux of  $\gamma$ -rays produced through nuclei de-excitation process dominates by an order of magnitude that resulting from  $\pi^0$  production and decay in collisions of nuclei with the ambient gas background.

(3) The presence of a significant neutrino signal from decay of neutrons produced in the course of the photo-disintegration is strongly contingent on the abundance of  ${}^4\text{He}$  in the source, mirroring its observed prevalence in cosmic rays. This compensates by an order of magnitude over its reduced photo-disintegration rate, and results in a  $\bar{\nu}_\mu$  signal at IceCube (after oscillation from  $\bar{\nu}_e$ ) comparable to the  $\nu_\mu$  signal from hadronic interactions (as noted previously, this is sufficient to establish a  $15\sigma$  discovery in 15 years of observation.) The ability of IceCube to measure flavor ratios can distinguish between these possibilities [118].

(4) For this model to succeed, a high efficiency is required for accelerating a low energy population of nuclei at the source to PeV energies. Thus, evidence for the model (such as a substantial suppression in the  $\gamma$ -ray spectrum below  $\sim 1$  TeV) could provide some insight into source dynamics.

(5) It is noteworthy that the contribution to the diffuse  $\gamma$ -ray flux component resulting from the interaction of extreme-energy cosmic ray nuclei with the background radiation fields permeating the universe [119] is well below the observed EGRET data [120] (for details see Ref. [17]).

In summary, the availability of new data in coming years in  $\gamma$ -ray, X-ray, neutrino and cosmic-ray sector experiments affords an outstanding opportunity for study of high energy processes in extreme environments. Care-

ful exploration of model implications will provide an important complementary role to these observations.

### Acknowledgments

We would like to thank Felix Aharonian, Gavin Rowell, and the HEGRA Collaboration for permission to reproduce Fig. 2. We would also like to thank Tom Paul, Subir Sarkar and Stefan Westerhoff for valuable discussions on the EeV (an)isotropy. We are indebted to the HiRes Collaboration for permission to make public their results on the anisotropy search around the Cygnus region. We are grateful to Rene Ong for comments and a careful reading of the manuscript. The research of LAA is supported by the University of Wisconsin-Milwaukee. JFB is supported by The Ohio State University and the NSF CAREER Grant No. PHY-0547102. HG is supported by the U.S. National Science Foundation (NSF) Grant No PHY-0244507. SPR is supported by the NASA Grant ATP02-000-0151 and by the Spanish Grant FPA2005-01678 of the MCT. TJW is supported by the U.S. Department of Energy Grant No. DE-FG05-85ER40226, by the NASA Grant ATP02-000-0151, and by a Vanderbilt University Discovery Award.

### Note added

In the accompanying *Letter* [17] we have adopted a more descriptive notation for some variables. Throughout this paper we use the traditional notation, which shortens the text length of the equations. The equivalences are:  $\gamma = \Gamma_A$ ,  $\epsilon' = \Gamma_A \epsilon$ ,  $\epsilon'_0 = \epsilon_\gamma^{\text{GDR}}$ ,  $\overline{E'}_{\gamma A} = \epsilon_\gamma^{\text{dxn}}$ ,  $E_\gamma = \epsilon_\gamma^{\text{LAB}}$ ,  $E = E_A^{\text{LAB}}$ ,  $\Gamma = \Gamma^{\text{GDR}}$ , and  $\sigma_0 = \sigma^{\text{GDR}}$ .

- 
- [1] F. A. Aharonian, Very high energy cosmic gamma radiation: A crucial window on the extreme universe, (Singapore: World Scientific Publishing, 2004); V. L. Ginzburg and S. I. Syrovatskii, The origin of Cosmic Rays, (New York: MacMillan, 1964); F. W. Stecker, Cosmic Gamma Rays (Baltimore: Mono 1971).
  - [2] The Hillas criterion states that the maximum attainable energy is limited by the fact that particles can only be accelerated in a region until their Larmor radius exceeds its size. A. M. Hillas, Ann. Rev. Astron. Astrophys. **22**, 425 (1984).
  - [3] M. Ahlers, L. A. Anchordoqui, H. Goldberg, F. Halzen, A. Ringwald and T. J. Weiler, Phys. Rev. D **72**, 023001 (2005) [arXiv:astro-ph/0503229].
  - [4] L. Anchordoqui, H. Goldberg and C. Nunez, Phys. Rev. D **71**, 065014 (2005) [arXiv:hep-ph/0408284].
  - [5] F. Abe *et al.* [CDF Collaboration], Phys. Rev. D **41**, 2330 (1990).
  - [6] I. V. Moskalenko, PhD Thesis, Moscow State University, Moscow, 1985.
  - [7] M. Samorski and W. Stamm, Astrophys. J. **268**, L17 (1983).
  - [8] R. C. Lamb, C. E. Fichtel, R. C. Hartman, D. A. Kniffen, and D. J. Thompson, Astrophys. J. Lett. **212**, L63 (1977).
  - [9] S. Danaher, D. J. Fegan, N. A. Porter, and T. C. Weekes, Nature **289**, 568 (1987); R. C. Lamb, C. P. Godfrey, A. A. Wheaton and T. Tümer, Nature **296**, 543 (1982).
  - [10] J. Lloyd-Evans, R. N. Coy, A. Lambert, J. Lapikens, M. Patel, R. J. Reid and A. A. Watson, Nature **305** (1983) 784.
  - [11] L. Anchordoqui, T. Paul, S. Reucroft and J. Swain, Int. J. Mod. Phys. A **18**, 2229 (2003) [arXiv:hep-ph/0206072].
  - [12] G. L. Cassiday *et al.*, Phys. Rev. Lett. **62**, 383 (1989).
  - [13] M. Teshima *et al.*, Phys. Rev. Lett. **64**, 1628 (1990).
  - [14] A. Borione *et al.* [CASA-MIA Collaboration], Phys. Rev. D **55**, 1714 (1997) [arXiv:astro-ph/9611117].
  - [15] F. Aharonian *et al.* [HEGRA Collaboration], Astron.

- Astrophys. **431**, 197 (2005) [arXiv:astro-ph/0501667].
- [16] M. J. Lang *et al.*, Astron. Astrophys. **423**, 415 (2004) [arXiv:astro-ph/0405513].
- [17] L. A. Anchordoqui, J. F. Beacom, H. Goldberg, S. Palomares-Ruiz, and T. J. Weiler, astro-ph/0611580.
- [18] L. Münch and W. W. Morgan, Astrophys. J. **118**, 161 (1953).
- [19] H. L. Johnson and W. W. Morgan, Astrophys. J. **119**, 344 (1954).
- [20] W. W. Morgan, A. B. Meinel and H. M. Johnson, Astrophys. J. **120**, 506 (1954); D. H. Schulte, Astrophys. J. **123**, 250 (1956); *ibid.* **124**, 530 (1956) and *ibid.* **128**, 41 (1958).
- [21] L. C. Lawrence and V. C. Reddish, Publ. R. Obs. Edinburgh, **3**, 275 (1965) and *ibid.* **5**, 111 (1965).
- [22] V. C. Reddish, L. C. Lawrence and N. M. Pratt, Publ. R. Obs. Edinburgh, **5**, 111 (1966).
- [23] V. C. Reddish, L. C. Lawrence and N. M. Pratt, Mon. Not. Roy. Astron. S. **136**, 428 (1967) and Publ. R. Obs. Edinburgh, **5**, 112 (1967).
- [24] N. R. Walborn, Astrophys. J. **180**, L35 (1973); K. Völcker, Astr. Astrophys. Suppl. **22**, 1 (1975); J. B. Hutchings, Publ. R. Obs. Edinburgh, **93**, 50 (1981); C. Leitherer, H. Hefele, O. Stahl and B. Wolf, Astron. Astrophys. **108**, 102 (1982).
- [25] J. Knödseder, Astron. Astrophys. **360**, 539 (2000). [arXiv:astro-ph/0007442].
- [26] F. Comerón, A. Pasquali, G. Rodighiero, V. Stanishev, E. De Filippis, B. López Martí, M. C. Gálvez Ortiz, A. Stankov and R. Gredel, Astron. Astrophys. **389**, 874 (2002).
- [27] M. M. Hanson, Astrophys. J. **597**, 957 (2003) [arXiv:astro-ph/0307540].
- [28] A. V. Torres-Dogden, M. Tapia and M. Carroll, Mon. Not. Roy. Astron. S. **249**, 1 (1991).
- [29] P. Massey and A. B. Thompson Astron. J. **101**, 4 (1991).
- [30] G. Meynet, A. Maeder, G. Schaeller, D. Schaerer and C. Charbonnel, Astron. Astrophys. **103**, 97 (1994).
- [31] J. Knödseder, M. Cerviño, J.-M. Le Duigou, G. Meynet, D. Schaerer and P. von Ballmoos, Astron. Astrophys. **390**, 945 (2002). [arXiv:astro-ph/0206045].
- [32] D. C. Abbott, J. H. Biegging and E. Churchwell, Astrophys. J. **250**, 645 (1981).
- [33] A. Herrero, L. J. Corral, M. R. Villamariz and E. L. Martin, Astron. Astrophys. **348**, 542 (1999).
- [34] H. J. Wendker, L. A. Higgs and T. L. Landecker, Astron. Astrophys. **241**, 551 (1991).
- [35] M. Parthasarathy, S. K. Jain and H. C. Bhatt, Astron. Astrophys. **266**, 202 (1992).
- [36] A. Pigulski and Z. Kolaczowski, Mon. Not. Roy. Astron. S. **298**, 753 (1998).
- [37] C. Leitherer, C. Robert and L. Drissen, Astrophys. J. **401**, 596 (1992).
- [38] T. A. Lozinskaya, V. V. Pravdikova and A. Finoguenov, Astron. Lett. **28**, 223 (2002) [arXiv:astro-ph/0203015].
- [39] G. Puehlofer, O. Bolz and N. Gotting [HEGRA Collaboration], Astropart. Phys. **20**, 267 (2003) [arXiv:astro-ph/0306123].
- [40] F. A. Aharonian *et al.* [HEGRA Collaboration], Astron. Astrophys. **393**, L37 (2002) [arXiv:astro-ph/0207528].
- [41] M. Merck, Ph.D. Dissertation, Ludwig-Maximilians University, Munich (1993); H. Krawczynski, Diplom Thesis, University of Hamburg, Hamburg (1995), available at <http://www-hegra.desy.de/publications.html>; Y. I. Neshpor *et al.*, Nuovo Cim. **19C**, 1385 (1996).
- [42] M. S. E. Roberts, R. W. Romani and N. Kawai, Astrophys. J. Suppl. **133**, 451 (2001) [arXiv:astro-ph/0012304].
- [43] R. K. Manchanda, V. F. Polcaro, L. Norci, F. Giovanelli, W. Brinkmann, H. D. Radecke, M. Manteiga, P. Persi and C. Rossi, Astron. Astrophys. **305**, 457 (1996); P. Benaglia, G. E. Romero, I. R. Stevens and D. F. Torres, Astron. Astrophys. **366**, 605 (2001). [arXiv:astro-ph/0010605].
- [44] Y. Butt *et al.*, Astrophys. J. **597**, 494 (2003). [arXiv:astro-ph/0302342]; Y. Butt, J. Drake, P. Benaglia, J. Combi, T. Dame, F. Miniati and G. Romero, Astrophys. J. **643**, 238 (2006) [arXiv:astro-ph/0509191].
- [45] R. C. Hartman *et al.* [EGRET Collaboration], Astrophys. J. Suppl. **123**, 79 (1999).
- [46] F. A. Aharonian and A. A. Atoyan, New Astron. Rev. **42**, 579 (1998).
- [47] J. Martí, J. M. Paredes and M. Peracaula, Astrophys. J. **545**, 939 (2000) and Astron. Astrophys. **375**, 476 (2001).
- [48] D. F. Torres, E. Domingo-Santamaria and G. E. Romero, Astrophys. J. **601**, L75 (2004) [arXiv:astro-ph/0312128].
- [49] L. Yao, E. R. Seaquist, N. Kuno and L. Dunne, Astrophys. J. **588**, 771 (2003) [Erratum-*ibid.* **597**, 1271 (2003)] [arXiv:astro-ph/0301511].
- [50] E. Domingo-Santamaria and D. F. Torres, Astron. Astrophys. **448**, 613 (2006) [arXiv:astro-ph/0510769].
- [51] R. Mukherjee, J. P. Halpern, E. V. Gotthelf, M. Eracleous and N. Mirabal, Astrophys. J. **589**, 487 (2003) [arXiv:astro-ph/0302130].
- [52] W. Bednarek, Mon. Not. Roy. Astron. Soc. **345**, 847 (2003) [arXiv:astro-ph/0307216].
- [53] Soon after this paper was submitted to the arXiv, a new finding on a possible weak radio counterpart in the vicinity of the source has been reported in, Y. M. Butt, J. A. Combi, J. Drake, J. P. Finley, A. Konopelko, M. Lister and J. Rodriguez, arXiv:astro-ph/0611731. This adds yet another dimension to the discussion of the nature of TeV J2032+4130.
- [54] V. V. Balashov, V. L. Korotkikh and I. V. Moskalenko, Moscow University Phy. Bull. **42**, 93 (1987); V. V. Balashov, V. L. Korotkikh and I. V. Moskalenko, Proc. 21st Int. Cosmic Ray Conf., Adelaide, Australia **2**, 416 (1990); S. Karakula, G. Kocielek, I. V. Moskalenko and W. Tkaczyk, Proc. 22nd Int. Cosmic Ray Conf. (Dublin) **1**, 536 (1991); S. Karakula, G. Kocielek, I. V. Moskalenko and W. Tkaczyk, Astrophys. J. Suppl. **92**, 481 (1994).
- [55] E. Hayward, Rev. Mod. Phys. **35**, 324 (1963); M. Danos and E. G. Fuller, Ann. Rev. Nucl. Part. Sci. **15**, 29 (1965); E. Hayward, NBS Monog. No. 118 (1970).
- [56] F. W. Stecker, Phys. Rev. **180**, 1264 (1969).
- [57] J. L. Puget, F. W. Stecker and J. H. Bredekamp, Astrophys. J. **205**, 638 (1976). The photodisintegration energy thresholds for all isotopes in the decay chain of  $^{56}\text{Fe}$  have been updated in, F. W. Stecker and M. H. Salamon, Astrophys. J. **512**, 521 (1999) [arXiv:astro-ph/9808110].
- [58] S. Karakula and W. Tkaczyk, Astropart. Phys. **1**, 229 (1993).

- [59] Evaluation of the Thomas-Reiche-Kuhn (TRK) dipole sum rule (for an isotope of charge  $Ze$  and  $N$  neutrons)  $\Sigma_d \equiv \int_0^\infty \sigma_A(\epsilon') d\epsilon' \simeq 59.8 \frac{NZ}{A}$  mb MeV gives, for  $^{56}\text{Fe}$ , 1020 mb-MeV for the left hand side, 22% larger than the right hand side.
- [60] L. A. Anchordoqui, M. T. Dova, L. N. Epele and J. D. Swain, *Phys. Rev. D* **57**, 7103 (1998) [arXiv:astro-ph/9708082].
- [61] R. M. Crocker, M. Fatuzzo, R. Jokipii, F. Melia and R. R. Volkas, *Astrophys. J.* **622**, 892 (2005) [arXiv:astro-ph/0408183]; D. Grasso and L. Maccione, *Astropart. Phys.* **24**, 273 (2005) [arXiv:astro-ph/0504323]; V. Cavasinni, D. Grasso and L. Maccione, *Astropart. Phys.* **26**, 41 (2006) [arXiv:astro-ph/0604004].
- [62] S. P. Lai, R. M. Crutcher, J. M. Girart and R. Rao, *Astrophys. J.* **566**, 925 (2002) [arXiv:astro-ph/0107322].
- [63] The factor  $9/(4R^2)$  is the result of calculating  $\int d^3\vec{r}_1 \int d^3\vec{r}_2 |\vec{r}_1 - \vec{r}_2|^{-2} (4\pi R^3/3)^{-2}$ , where  $\vec{r}_1$  is the position of a star and  $\vec{r}_2$  is the position of an observer (the position of the reaction) in a region  $R$  with uniformly distributed sources.
- [64] W. L. Waldron, J. P. Cassinelli, N. A. Miller, J. J. MacFarlane and J. C. Reiter, *Astrophys. J.* **616**, 542 (2004) [arXiv:astro-ph/0407376].
- [65] W. D. Vacca, C. D. Garmany and J. M. Shull, *Astrophys. J.* **460**, 914 (1996).
- [66] It should be noted that for an ambient gas density  $n_{\text{tot}} \approx 0.1 \text{ cm}^{-3}$  the interaction time for nucleus-proton collisions is  $1.5 \times 10^8$  yr, more than two orders of magnitude larger than the photo-disintegration time scale. This estimate is based on a hadronic cross section,  $\sigma_{\text{Fep}} \sim A^{0.75} \sigma_{pp} \approx 7 \times 10^{-25} \text{ cm}^2$ .
- [67] The  $47/(4R_{\text{out}}^2)$  factor is the result of calculating  $\int d^3\vec{r}_1 \int d^3\vec{r}_2 \rho(r_1) |\vec{r}_1 - \vec{r}_2|^{-2} (N_O + N_B)^{-1} (4\pi r^3/3)^{-1}$ , where  $\rho(r_1)$  is the density of stars in a region of radius  $R_{\text{out}}$  and the reaction occurs in a region of radius  $r$ .
- [68] V. L. Korotkikh, E. L. Yadrovskii and V. V. Varlamov, Nuclear Physics Institute, Moscow State University, Preprint No. 88-33/54 (1988); I. V. Moskalenko and O. V. Fotina, *Yad. Fiz.* **49**, 1623 (1989).
- [69] J. T. Caldwell, S. C. Fultz and R. L. Bramblett, *Phys. Rev. Lett.* **19**, 447 (1967).
- [70] J. E. Carson, arXiv:astro-ph/0610960.
- [71] J. R. Horandel, arXiv:astro-ph/0508014; T. Antoni *et al.* [KASCADE Collaboration], *Astropart. Phys.* **24**, 1 (2005) [arXiv:astro-ph/0505413].
- [72] L. A. Anchordoqui, H. Goldberg, F. Halzen and T. J. Weiler, *Phys. Lett. B* **593**, 42 (2004) [arXiv:astro-ph/0311002].
- [73] <http://www.nndc.bnl.gov/nudat2/> See also, D. R. Tilley, H. R. Weller and H. H. Hasan, *Nucl. Phys. A* **474**, 1 (1987).
- [74] J. Ahrens *et al.* [IceCube Collaboration], *Astropart. Phys.* **20**, 507 (2004) [arXiv:astro-ph/0305196].
- [75] J. Ahrens *et al.* [IceCube Collaboration], *Nucl. Phys. Proc. Suppl.* **118**, 388 (2003) [arXiv:astro-ph/0209556].
- [76] M. C. Gonzalez-Garcia, F. Halzen and M. Maltoni, *Phys. Rev. D* **71**, 093010 (2005) [arXiv:hep-ph/0502223].
- [77] L. A. Anchordoqui, H. Goldberg, M. C. Gonzalez-Garcia, F. Halzen, D. Hooper, S. Sarkar and T. J. Weiler, *Phys. Rev. D* **72**, 065019 (2005) [arXiv:hep-ph/0506168].
- [78] M. C. Gonzalez-Garcia, *Phys. Scripta* **T121**, 72 (2005) [arXiv:hep-ph/0410030]; K. Miknaitis [SNO Collaboration], arXiv:hep-ex/0505071. The oscillation parameters derived in Ref. [77] are equivalently to those given in T. Schwetz, *Phys. Scripta* **T127**, 1 (2006) [arXiv:hep-ph/0606060].
- [79] M. Ackermann [AMANDA Collaboration], *Astropart. Phys.* **22**, 127 (2004) [arXiv:astro-ph/0405218].
- [80] M. Honda, T. Kajita, K. Kasahara and S. Midorikawa, *Phys. Rev. D* **70**, 043008 (2004) [arXiv:astro-ph/0404457].
- [81] L. V. Volkova, *Sov. J. Nucl. Phys.* **31**, 784 (1980) [*Yad. Fiz.* **31**, 1510 (1980)].
- [82] P. Gondolo, G. Ingelman and M. Thunman, *Astropart. Phys.* **5**, 309 (1996) [arXiv:hep-ph/9505417].
- [83] A. Kappes, J. Hinton, C. Stegmann and F. A. Aharonian, arXiv:astro-ph/0607286.
- [84] T. K. Gaisser, *Cosmic Rays and Particle Physics*, Cambridge, UK: University Press (1990).
- [85] M. L. Costantini and F. Vissani, *Astropart. Phys.* **23**, 477 (2005) [arXiv:astro-ph/0411761].
- [86] L. A. Anchordoqui, H. Goldberg, F. Halzen and T. J. Weiler, *Phys. Lett. B* **600**, 202 (2004) [arXiv:astro-ph/0404387].
- [87] M. D. Kistler and J. F. Beacom, *Phys. Rev. D* **74**, 063007 (2006) [arXiv:astro-ph/0607082].
- [88] See Table 24.1 in W. M. Yao *et al.* [Particle Data Group], *J. Phys. G* **33**, 1 (2006).
- [89] The ratio of  $\sim 100$  is taken from Table 24.1 of W. M. Yao *et al.*, Ref. [88], and is at an energy of 10.4 GeV/nucleon. This ratio is expected to extrapolate to higher energies as long as the cosmic rays are trapped in the Galaxy, perhaps up to 10 TeV/nucleon. In order to account for the HEGRA data, the accelerative process requires injection from the nuclei population at energies 2-3 orders of magnitude lower than 1 PeV/nucleon (see discussion following Eq.(23)), where we expect this ratio to hold.
- [90] F. W. Stecker, *Cosmic Gamma Rays*, Baltimore: Mono Book Co. (1971).
- [91] F. W. Stecker, *Astrophys. Sp. Sci.* **4**, 377 (1970).
- [92] G. D. Badhwar, S. A. Stephens and R. L. Golden, *Phys. Rev. D* **15**, 820 (1977); S. A. Stephens and G. D. Badhwar, *Astrophys. Sp. Sci.* **76**, 213 (1981).
- [93] S. R. Blattnig, S. R. Swaminathan, A. T. Kruger, M. Ngom and J. W. Norbury, *Phys. Rev. D* **62**, 094030 (2000) [arXiv:hep-ph/0010170].
- [94] C. D. Dermer, *Astron. Astrophys.* **157**, 223 (1986).
- [95] I. V. Moskalenko and A. W. Strong, *Astrophys. J.* **493**, 694 (1998) [arXiv:astro-ph/9710124].
- [96] P. Blasi and S. Colafrancesco, *Astropart. Phys.* **122**, 169 (1999) [arXiv:astro-ph/9905122].
- [97] F. A. Aharonian and A. M. Atoyan, *Astron. Astrophys.* **362**, 937 (2000) [arXiv:astro-ph/9803091].
- [98] T. Kamae, T. Abe and T. Koi, *Astrophys. J.* **620**, 244 (2005) [arXiv:astro-ph/0410617]. T. Kamae, N. Karlsson, T. Mizuno, T. Abe and T. Koi, *Astrophys. J.* **647**, 692 (2006) [arXiv:astro-ph/0605581].
- [99] E. Domingo-Santamaria and D. F. Torres, *Astron. Astrophys.* **444**, 403 (2005) [arXiv:astro-ph/0506240].
- [100] S. R. Kelner, F. A. Aharonian and V. V. Bugayov, *Phys. Rev. D* **74**, 034018 (2006) [arXiv:astro-ph/0606058].
- [101] R. S. Fletcher, T. K. Gaisser, P. Lipari and T. Stanev, *Phys. Rev. D* **50**, 5710 (1994).
- [102] A. M. Lebedev, S. A. Slavatinskii and B. V. Tolkachev,

- Sov. Phys. JETP **19**, 1452 (1963).
- [103] N. Hayashida *et al.* [AGASA Collaboration], *Astropart. Phys.* **10**, 303 (1999) [arXiv:astro-ph/9807045]; M. Teshima *et al.*, Proc. 27th Int. Cosmic Ray Conf. (ICRC 2001), Hamburg, Germany, 337 (2001).
- [104] D. J. Bird *et al.* [Fly's Eye Collaboration], *Astrophys. J.* **511**, 739 (1999) [arXiv:astro-ph/9806096].
- [105] J. Abraham *et al.* [Pierre Auger Collaboration], *Astropart. Phys.* (in press) [arXiv:astro-ph/0607382].
- [106] T. Antoni *et al.* [KASCADE Collaboration], *Astrophys. J.* **604**, 687 (2004) [arXiv:astro-ph/0312375].
- [107] M. A. Lawrence, D. C. Prosser and A. A. Watson, *Phys. Rev. Lett.* **63**, 1121 (1989).
- [108] M. Ave, J. Knapp, J. Lloyd-Evans, M. Marchesini and A. A. Watson, *Astropart. Phys.* **19**, 47 (2003) [arXiv:astro-ph/0112253].
- [109] M. A. Lawrence, R. J. O. Reid and A. A. Watson, *J. Phys. G* **17**, 733 (1991).
- [110] R. U. Abbasi *et al.* [HiRes Collaboration], arXiv:astro-ph/0507663.
- [111] S. Westerhoff and C. B. Finley [HiRes Collaboration], arXiv:astro-ph/0507574.
- [112] R. U. Abbasi *et al.* [HiRes Collaboration], *Astrophys. J.* **623**, 164 (2005) [arXiv:astro-ph/0412617].
- [113] HiRes Collaboration, private communication.
- [114] J. Abraham *et al.* [Pierre Auger Collaboration], *Nucl. Instrum. Meth. A* **523**, 50 (2004).
- [115] C. D. Wilson, C. E. Walker and M. D. Thornley, *Astrophys. J.* **483**, 210 (1997) [arXiv:astro-ph/9701245].
- [116] J. Goodman, "Recent Results on the Cygnus Region from Milagro," talk given at TeV Particle Astrophysics II, (Madison, August 2006). To be published in *J. Phys. Conf. Ser.*
- [117] M. Amenomori *et al.* [Tibet AS-gamma Collaboration], *Science* **314**, 439 (2006) [arXiv:astro-ph/0610671].
- [118] It is worth noticing that the  $\bar{\nu}$   $\beta$ -beam provides a unique discriminator of very long baseline neutrino-mixings, and therefore can serve as a extremely sensitive probe of new physics in the electroweak sector. See, e.g., J. F. Beacom, N. F. Bell, D. Hooper, S. Pakvasa and T. J. Weiler, *Phys. Rev. Lett.* **90**, 181301 (2003) [arXiv:hep-ph/0211305]; *Phys. Rev. D* **69**, 017303 (2004) [arXiv:hep-ph/0309267]; J. F. Beacom, N. F. Bell, D. Hooper, J. G. Learned, S. Pakvasa and T. J. Weiler, *Phys. Rev. Lett.* **92**, 011101 (2004) [arXiv:hep-ph/0307151]; H. Athar, M. Jezabek and O. Yasuda, *Phys. Rev. D* **62**, 103007 (2000) [arXiv:hep-ph/0005104]; L. Anchordoqui and F. Halzen, *Annals Phys.* **321**, 2660 (2006) [arXiv:hep-ph/0510389]. See also Ref. [77].
- [119] M. A. Malkan and F. W. Stecker, *Astrophys. J.* **496**, 13 (1998) [arXiv:astro-ph/9710072]; F. W. Stecker, M. A. Malkan and S. T. Scully, *Astrophys. J.* **648**, 774 (2006) [arXiv:astro-ph/0510449]. See also, M. Hauser and E. Dwek, *Ann. Rev. Astron. Astrophys.* **39**, 249 (2001) [arXiv:astro-ph/0105539].
- [120] P. Sreekumar *et al.* [EGRET Collaboration], *Astrophys. J.* **494**, 523 (1998) [arXiv:astro-ph/9709257]; A. W. Strong, I. V. Moskalenko and O. Reimer, *Astrophys. J.* **613**, 956 (2004) [arXiv:astro-ph/0405441].